LUND UNIVERSITY

Epitaxial Growth, Processing and Characterization of Semiconductor Nanostructures

Borgström, Magnus

2003

Link to publication

Citation for published version (APA):
Borgström, M. (2003). *Epitaxial Growth, Processing and Characterization of Semiconductor Nanostructures*. Division of Solid State Physics, Department of Physics, Lund University, Box 118, SE-221 00 Lund, Sweden,.

Total number of authors:
1

General rights
Unless other specific re-use rights are stated the following general rights apply:
Copyright and moral rights for the publications made accessible in the public portal are retained by the authors and/or other copyright owners and it is a condition of accessing publications that users recognise and abide by the legal requirements associated with these rights.
• Users may download and print one copy of any publication from the public portal for the purpose of private study or research.
• You may not further distribute the material or use it for any profit-making activity or commercial gain
• You may freely distribute the URL identifying the publication in the public portal

Read more about Creative commons licenses: https://creativecommons.org/licenses/

Take down policy
If you believe that this document breaches copyright please contact us providing details, and we will remove access to the work immediately and investigate your claim.

LUND UNIVERSITY

PO Box 117
221 00 Lund
+46 46-222 00 00

Download date: 07. Oct. 2022

Epitaxial growth, processing, and characterization of semiconductor nanostructures

Magnus Borgström

LUND INSTITUTE OF TECHNOLOGY
Lund University

Division of Solid State Physics
Sweden 2003

Akademisk avhandling som för avläggande av teknologie doktorsexamen vid tekniska fakulteten vid Lunds Universitet offentligen kommer att försvaras i Fysiska institutionens föreläsningssal B, Sölvegatan 14, fredagen den 28 November 2003, kl. 10.15.

Division of Solid State Physics
Lund University
Box 118
S-221 00 Lund
Sweden

© Magnus Borgström, 2003
ISBN 91-628-5876-9
KFS AB, Lund 2003
Printed in Sweden

Abstract

This thesis deals with the growth, processing and characterization of nano-sized structures, *eg.*, self-assembled quantum dots and nano-wires. Such structures are promising candidates for the realization of nano-scale electronic and optical devices, like for instance single electron transistors, resonant tunneling devices, and single photon emitters. For such purposes, the main focus of this work has been on the controlled growth of self-assembled quantum dots.

For epitaxy, which is the fundament of this work, low-pressure metal organic vapor phase epitaxy (MOVPE) and ultra high vacuum chemical vapor deposition (UHV-CVD) were used. The structures grown were composed of III/V materials, and SiGe/Si was used for some experiments.

For the first group of structures, fundamental investigations on quantum dot growth enabled *in-situ* growth of InAs/InP self-assembled quantum dot samples in MOVPE. These studies were carried out on freestanding as well as epitaxially overgrown dots. Topography and photo-luminescence were measured with atomic force microscope (AFM) and Fourier transform infrared spectroscopy (FTIR) respectively. InAs/InP low-density quantum dot samples were grown in single or multiple layers, suitable for electrical measurements. These structures were studied by electrical characterization (IV), transmission electron microscopy (TEM), and cross sectional scanning tunneling microscopy (STM). Resonant tunneling through these quantum dots was observed, with peak-to-valley ratios as high as 1300 and negative differential resistance up to a point above the temperature of liquid nitrogen.

For the second, more complex, group of structures, patterns on semiconductor surfaces were created, either by electron beam lithography and wet chemical etching, or by the partial overgrowth of electron beam induced carbonaceous material. Spatially ordered growth of III/V and SiGe/Si quantum dots on such patterns was studied by AFM. For the InAs/InP system, conditions were found for which dots could be grown selectively in the patterns by the use of As-P exchange reactions. For the SiGe/Si system, commonly quadruples of islands were observed around each pit.

The third group of structures was grown from size selected gold particles, deposited in-house in an aerosol machine, or from Au colloids that were dispersed on the semiconductor surface. These gold particles enabled vapor-liquid-solid (VLS) growth of highly anisotropic one-dimensional structures that were characterized by scanning electron microscopy.

Contents

Preface iv

List of papers vi

1 Properties of low-dimensional structures 1

1.1 Introduction 1
1.2 Energy bands 1
1.3 Band gap engineering 2
1.3.1 Resonant tunneling through quantum dots 4
1.3.2 Structure proposed 6

2 Epitaxy 7

2.1 Introduction 7
2.2 CVD 7
2.2.1 UHV-CVD 9
2.2.2 MOVPE 9
2.3 Growth modes 10
2.4 Self-assembled island formation 12
2.4.1 Dot size, homogeneity, and density 13
2.4.2 Interface reactions 14
2.5 Vapor-liquid-solid growth 15

3 Site control 19

3.1 Introduction 19
3.2 Modification of the surface chemical potential 19
3.3 *In-situ* spontaneously ordered dot growth 21
3.4 Lateral positioning of dots by surface patterning 22
3.4.1 Electron beam induced carbon deposition for patterning 28
3.5 Vertical stacking of quantum dots 30

4. Imaging techniques 35

4.1 Introduction 35
4.2 Scanning probe microscopy 35
4.3 Electron beam microscopy 37

5 Summary of papers 39

Paper I, II, and VII (*In-situ* growth of self-assembled quantum dots) 39
Paper III, V and VI (resonant tunneling through self-assembled quantum dots) 40
Paper IV, VIII, and IX (lateral site control of self assembled quantum dots structures) 42
Paper X, (vertical stacking of quantum dots) 43
Paper XI, and XII (growth of one dimensional nano-whiskers) 43

References 45

Preface

This thesis is based on epitaxial growth, processing and characterization of nano-structures. The scope of the work is summarized in the enclosed papers, whereas the introductory part is intended to introduce the area of research, the experimental techniques, and the characterization tools to a non-expert, *e.g.*, a PhD student who has recently entered the field of nano-physics, or someone plainly interested in the field. The introduction will also provide an overview of the scientific result obtained within the framework of the thesis, and will partly overlap with the included papers.

The text is organized into five parts. The first part describes the basic properties of semiconductors and low dimensional structures. The second part gives an introduction to the principle of epitaxy, the fundament of this work. The third part treats the subject of site-controlled growth, and in the fourth part an introduction to characterization tools that have been used during the work is given. Finally the fifth part gives a short summary of the papers enclosed.

During my time at the department, I have been given the opportunity of participation in a creative environment, which I'm grateful for. I have seen a great challenge in the field of nano-science. Never could I have guessed though, that so much time was going to be spent simply trying to clean samples. Epitaxy is very sensitive process, and any contamination will inevitably ruin the growth.

There are a vast number of people who have assisted me during my scientific work. First of all I would like to acknowledge my supervisors: Prof. Werner Seifert and Prof. Lars Samuelson, at Solid State Physics. Werner has been a roommate for most of the time, and has as such become a very good friend. We have worked in close cooperation, and have had uncountable interesting discussions during the course of this work, which has benefited enormously from Werners great knowledge about epitaxy and his never-ending ideas. Lars has always been an infinite source of inspiration and keen on sharing his visions about nano physics.

I want to thank Dr. Jonas Johansson for being friend and mentor. During every day work I have been cooperating with several persons. I am glad to have had the chance to know them: Tomas Bryllert, Dr. Boel Gustafson, and Dr. Lars-Erik Wernersson, on IV-characterization, Dr. Torsten Sass on TEM, Thomas Mårtensson, Dr. Ines Pietzonka, and Niklas Sköld on MOVPE, Anders Mikkelsen on STM, Dr. Lars Landin, and Dr. Håkan Petterson, on photoluminescence and DLTS measurements, Dr. Jonas Ohlsson, and Ann Persson for inspiring whisker

meetings, Dr. Knut Deppert, Martin Karlsson and Brent Wacaser dominating the aerosol machine. Martin Persson is acknowledged for many interesting discussions during long workdays, he is a many facetted guy. Thank you Vilma Zela for UHV-CVD growth, nice coffee breaks, and discussions about science and life.

I am very happy to have spent some time at Pontifícia Universidade Católica do Rio de Janeiro. Thank you Prof. Patrícia Lustoza de Souza for making this trip possible, and for your friendliness and support. In addition to further insights in MOVPE engineering skills and growth, I gained great friends in the department, especially in Prof. Maurício Pamplona Pires with whom I worked in close collaboration, and Amália Regina de Oliveira who kept an eye on me as I wandered off into the more unsafe regions of the city.

I acknowledge the people who have helped me with processing of any kind, Erik Lind, Dr. Ivan Maximov, Ewa-Lena Sarwe, Dr. Ivan Shorubalko, and Lena Timby. I also wish to thank Bengt Bengtsson, Sören Jeppesen, Peter Johansson, Tord Stjernholm, and Lars-Göran Wennerberg for their assistance with engineering skills, sometimes beyond what anyone could expect. Whenever I had any bureaucratic problems, Mona Hammar came to rescue, thank you.

I would like to thank my family for invaluable support and love; you have always been there. Sincere thanks to all of my non-physicist friends who have given me many good times and fine discussions. Finally I would like to thank Andréa who has been a part of my life since Rio, you are the best.

Magnus Borgström, Lund 2003.

List of papers

The thesis is based on the following papers, which span over three areas of research: *i)* Fundamental studies on the epitaxial growth of InAs/InP quantum dots in MOVPE, by the use of characterization tools like atomic force microscope, photoluminescence, and electrical measurements. *ii)* The development of a method for site-controlled growth of quantum dots on patterned surfaces. *iii)* Fundamental studies on nanometer-sized whiskers in MOVPE that present promising results of a recently initiated research project.

I L. Landin, M. Borgström, M. Kleverman, M.-E. Pistol, L. Samuelson, W. Seifert, X. H: Zhang, *"Optical investigations of InAs/InP quantum dots at different temperatures and under electric field",* Thin Solid Films 364 (2000) 161

II M. Borgström, J. Johansson, L. Landin, W. Seifert, "Effects of substrate doping and surface roughness on self-assembling InAs/InP quantum dots", Applied Surface Science 165 (2000) 241

III M. Borgström, T. Bryllert, T. Sass, B. Gustafson, L.-E. Wernersson, W. Seifert, L. Samuelson, *"High peak-to-valley ratios observed in stacked InAs/InP resonant tunneling quantum dot stacks",* Applied Physics Letters 78 (2001) 3232

IV M. Borgström, J. Johansson, L. Samuelson, W. Seifert, "*Electron beam pre-patterning for site-control of self-assembled quantum dots*", Applied Physics Letters 78 (2001) 1367

V. T. Bryllert, M. Borgström, T. Sass, B. Gustafson, L. Landin, L.-E. Wernersson, W. Seifert, L. Samuelson, *"Designed emitter states in resonant tunneling through quantum dots"*, Applied Physics Letters 80 (2002) 2681

VI T. Bryllert, M. Borgström, L.-E. Wernersson, W. Seifert, L. Samuelson, *"Transport through an isolated artificial molecule formed from stacked self-assembled quantum dots"*, Applied Physics Letters 82 (2003) 2655

VII. M. Borgström, T. Bryllert, T. Sass, L.-E. Wernersson, L. Samuelson, W. Seifert, *"Site-control of InAs quantum dots on a patterned InP surface: As/P exchange reactions",* Journal of Crystal Growth 240 (2003) 310

VIII. M. Borgström, M. P. Pires, T. Bryllert, S. Landi, W. Seifert, P. L. Souza, *"InAs quantum dots grown on InAlGaAs lattice matched to InP"*, Journal of Crystal Growth 252 (2003) 481

IX. M. Borgström, V. Zela, W. Seifert, "Arrays of Ge islands on Si(001) grown by means of electron-beam pre-patterning", Nanotechnology 14 (2003) 1

X. M. Borgström, K. Deppert, L. Samuelson, W. Seifert, *"Size- and shape-controlled GaAs nano-whiskers grown by MOVPE, a growth study",* Journal of Crystal Growth, in press

XI. T. Mårtensson, M. Borgström, B. J. Ohlsson, W. Seifert, L. Samuelson, *"Fabrication of single-seeded nanowire arrays by vapor-liquid-solid growth",* Nanotechnology, in press

XII M. Borgström, A. Mikkelsen, L. Ouattara, E. Lundgren, L. Samuelson, W. Seifert, *"Spontaneous InAs quantum dot nucleation at strained InP/GaInAs interfaces"*, Applied Physics Letters, submitted

The following papers are not included in the thesis due to an overlap in contents, or a content that goes beyond the scope of this thesis.

i L.-E. Wernersson, M. Borgström, B. Gustafson, A. Gustafsson, L. Jarlskog, J.-O. Malm, A. Litwin, L. Samuelson, W. Seifert, *"MOVPE overgrowth of metallic features for realisation of 3D metal semiconductor quantum devices",* Journal of Crystal Growth 221 (2000) 704

ii L. Jarlskog, L.-E. Wernersson, M. Borgström, W. Seifert, L. Samuelson, *"Facet formation and overgrowth of sub-µm W-patterns on GaAs(001) surfaces",* Journal of Crystal Growth 222 (2001) 534

iii L.-E. Wernersson, B. Gustafson, A. Gustafson, M. Borgström, I. Pietzonka, T. Sass, W. Seifert, L. Samuelson, *"Thin layers of GaInP, GaP and GaAsP in metalorganic vapour phase epitaxy-grown resonant tunnelling diodes"* Applied Surface Science 190 (2001) 252

iv M. Borgström, T. Bryllert, B. Gustafson, J. Johansson, T. Sass, L.-E. Wernersson, W. Seifert, and L. Samuelson, *"Electron beam pre-patterning for site-control of self-assembled InAs quantum dots on InP surfaces"*, Journal of Electronic Materials 30 (2001) 482

v L.-E. Wernersson, M. Borgström, B. Gustafson, A. Gustafsson, I. Pietzonka, M.-E. Pistol, T. Sass, W. Seifert, L. Samuelson, *"Metalorganic vapor phase epitaxy-grown GaP/GaAs/GaP and GaAsP/GaAs/GaAsP n-type resonant tunnelling diodes",* Applied Physics Letters 80 (2002) 1841

vi T. Sass, I. Pietzonka, M. Borgström, B. Gustafson, L.-E. Wernersson, W. Seifert, *"Strain in GaP/GaAs and GaAs/GaP resonant tunelling heterostructures",* Journal of Crystal Growth 248 (2003) 375

vii M. Borgström, V. Zela, W. Seifert, *"Quadruples of Ge dots grown on patterned Si surfaces",* Journal of Crystal Growth, in press

1 Properties of low-dimensional structures

1.1 Introduction

Solid-state materials can be grouped into three classes, insulators, semiconductors and conductors. The study of semiconductor materials began in the early nineteenth century [1]. Over the years, many semiconductor materials have been studied, while Si has been, and remains, the dominant material, mainly due to the high quality silicon dioxide, which is a very good insulator that can be thermally grown on silicon. In addition, silicon in the form of silica and silicates comprises 25% of the earth's crust, which makes the material very cheap in comparison to other alternatives [2]. However, many so-called compound semiconductors that consist of two or more elements have optical and electrical properties that are absent in silicon, something that has triggered intense research for more expensive materials as well, like for instance, GaAs and InP. These are III-V materials that have direct band gaps, which from an application point of view means that they are excellent candidates for light emitting devices. Depending on what materials being used, different wavelengths of emitted light can be obtained. Recently, in order to reach wavelengths corresponding to blue light, GaN has been employed, and by combining wavelengths from more than one source, white light can be obtained [3].

For electrical purposes, the invention of the transistor in 1947 [4,5] was the beginning of a new era in applied physics. In 1965, Gordon Moore made a famous observation, which has later been called "Moore's Law". That was four years after the first planar integrated circuit had been presented. In his original paper, Moore [6] observed that the number of components (*e.g.*, transistors) on a chip roughly doubled every year, and predicted that this trend would continue. Companies have so far managed to follow this "rule" by downscaling the components, *i.e.*, enabling a higher density of components. The physics for the large and the smaller components has remained the same. At some point, where the layers become very thin, the physics change though, and quantum mechanical effects need to be taken into account.

1.2 Energy bands

What makes the semiconductor materials so attractive is that the semiconductor can behave as an insulator as well as a conductor. For an isolated atom, the

electrons can have discrete energy levels only. For N atoms, the properties are given by their collective behavior. The chemical bonds between N atoms in a semiconductor are essentially of covalent character, where each atom contributes to the covalent bonds with its own valence electrons. In contrast to the atom where the valence electron occupy a discrete energy state, the electrons in the semiconductor must occupy a certain energy range, due to the Pauli exclusion principle. The electrons in the covalent bonds will therefore form an energy band known as the valence band. A situation where all the electrons are in the valence band is the ground state of the semiconductor, and then it is, in principle, nothing more than an isolator.

The first band above the valence band is called the conduction band, and is corresponding to the first excited state for an electron orbiting an atom. Electrons can be excited from the valence band to the conduction band by, for instance, thermal energy or photon absorption. Excited electrons may be driven through the empty electron states in the conduction band by an external applied bias, and the semiconductor then shows the properties of a conductor. The energy difference between the maximum energy in the valence band and the minimum energy in the conduction band is called the band gap, where no electron states are present.

1.3 Band gap engineering

In bulk crystals, the excited electrons in the conduction band or the holes in the valence band are allowed to move freely in all three dimensions. Since the energy bands are material dependent, offsets in the bands will form when different materials are put together in a hetero-junction. If a tentative junction has the conduction band edge of the first material higher than in the second material, and the valence band of the first material is lower than in the second material, then it is a type I hetero-junction [7].

In figure 1, the schematics of a type I hetero-junction is shown; the difference between a) and b) in the figure is the thickness of the material with lower band gap. Electrons diffuse to lower lying electron states, and will therefore fall into the low-energy gap. If the material is thin enough, the electrons can no longer move freely in the material but the wave nature of the electron needs to be taken into account. As a result, a new set of electron states will be introduced, which is illustrated in figure 1b). These states can be obtained by a quantum mechanical treatment, using a one-dimensional particle in box model. In such a quantum well, the electrons may move freely in two dimensions, in the plane of the quantum well, but in the z-direction the movement is quantized. If a narrow wire is

embedded in high band gap material, the electrons can move in one dimension only and the object is a quantum wire. In a quantum dot, electrons within the structure have no freedom of motion in any direction and the structure is fully quantized. Since the electronic structure of the quantum dot, with discrete energy levels, is very similar to that of the atom, they are often called artificial atoms.

The first quantum dots were realized by lithography and etching [8,9], whereas nowadays spontaneous processes for forming quantum dots are the most frequently occurring. Recently, many reports have been published with the focus on *in-situ* epitaxial growth of coherent quantum dots, which exhibit defect free interfaces, thus avoiding surface states and dislocations in the active structure.

By the use of such quantum dots, and band gap engineering, completely new functionalities may arise. For instance, single photon sources for quantum cryptography, quantum dot lasers, or single photon detectors on the optical side, single electron transistors, resonant tunneling diodes, or quantum cellular automata on the electronic side. During the work of this thesis, for instance, the quantum dots have been put to use in resonant tunneling structures.

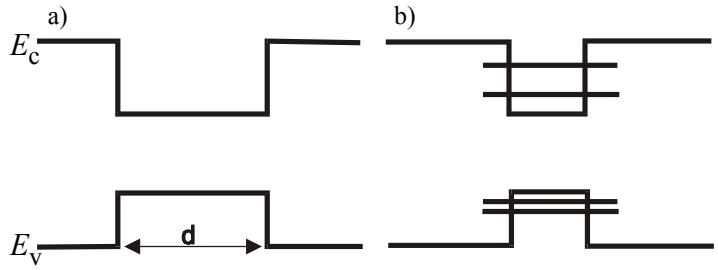

Fig 1 Schematics of type I hetero-junctions, a) d >>100 nm b) d << 100 nm, causing the formation of quantized electron states within the quantum well. By viewing the structure as a particle in a box problem with infinite walls, the solution to the Schrödinger equation gives the quantized electron energies, $E=\hbar^2\pi^2n^2/(2md^2)$, where n is an integer, 1,2,3…and m is the effective mass of the particle. The electron wave functions are given by sine waves, $\psi(x)=A\sin(n\pi x/d)\ 0 \leq x \leq d$, where A is the normalization constant. When the barriers are finite, the wave function will decay exponentially inside the barriers instead of ending abruptly.

1.3.1 Resonant tunneling through quantum dots

Resonant tunneling was first demonstrated in 1974 by Chang *et al.* [11] using a double barrier structure that was formed by embedding two slices of high band gap material, AlGaAs, in lower band gap material, GaAs. In figure 2, the schematics of a resonant tunneling structure are shown. Intuitively, resonant tunneling can be understood as an increased tunneling probability for electrons that have the same energy as the eigenstates localized between the barriers. An applied potential is assumed to fall entirely over the active structure. At zero applied bias voltage no current flows through the system, since the total barrier thickness is too large, unless the thermal energy is high enough so that electrons may pass over the

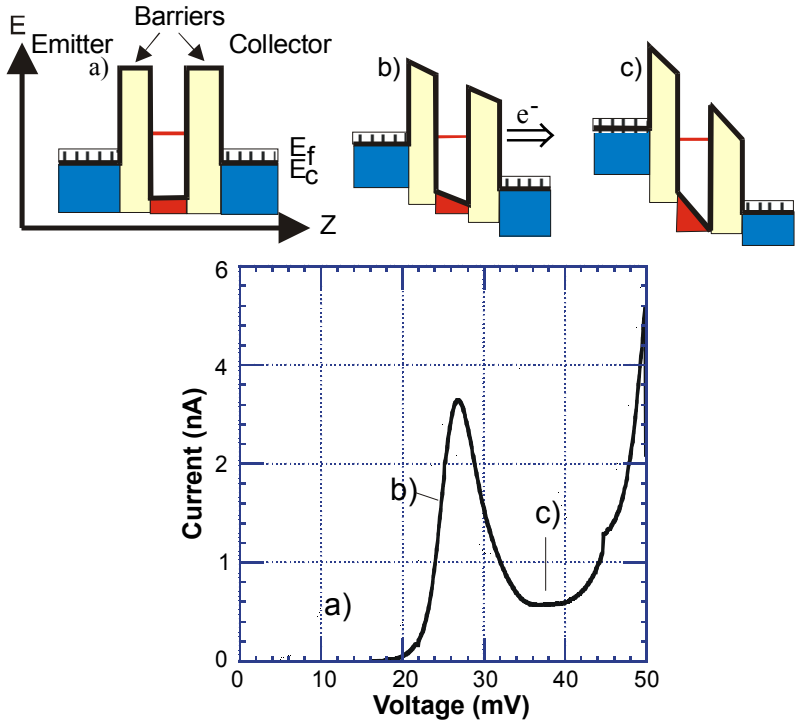

Fig 2 Schematic band diagram of a double barrier resonant tunneling structure. a) Before resonance, b) at resonance, and c) after resonance. The IV-diagram used to illustrate resonant tunneling shows the results of one of our first working resonant tunneling diodes [10]. The transport occurs through a dot in a single layer of low-density InAs quantum dots (≈1 μm^{-2}) in InP potential barriers. The structure was embedded in GaInAs emitter and collector.

barrier. At a certain point of voltage, the Fermi level [2] on the left side of the junction (Fig. 2) is aligned with the energy level in the dot. Due to the wave nature of the electrons, incident electrons with energy corresponding to the electron state in the dot now have a finite transmission probability through the structure to available electron states on the collector side, and can contribute to a current flow. This phenomenon is called resonant tunneling. When a large enough bias is applied, so that the resonant state falls below the conduction band edge in the emitter, tunneling is prohibited once again and a sharp drop in the IV-characteristics occurs. This is the region of negative-differential-resistance (NDR), and as a consequence, the IV-characteristics of such a device is non-ohmic.

Several groups have studied resonant tunneling through self-assembled quantum dots [14,15], usually with thousands of dots beneath a contact. For our studies on resonant tunneling we have used low density, about 1μm^{-2}, InAs quantum dots embedded in InP barriers [10,13,16]. By etching mesas, with

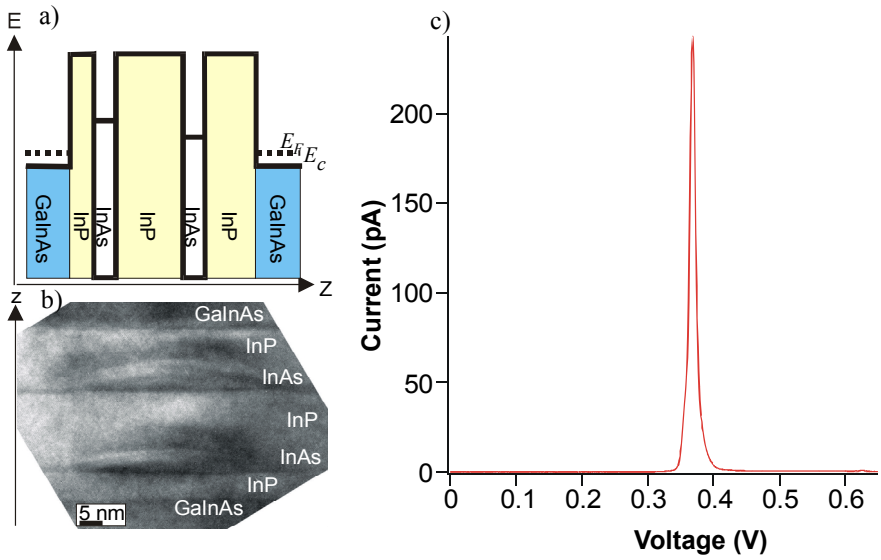

Fig 3 a) Schematic band diagram of an InAs/InP triple barrier quantum dot resonant tunneling diode. b) Transmission electron microscope image of the structure grown. The structure grown was 5nm InP/0.3 ML InAs/15 nm InP, 0.3 ML InAs, and 12 nm InP, all embedded in GaInAs. Note that the upper dot is slightly larger than the lower one, which explains the IV-characteristics of the device [12]. c) The electron ground states of the dots can align at a certain applied bias, resulting in a sharp resonant feature with peak-to-valley ratio as high as 1300, at a temperature of 4 K [13].

micrometer-sized contacts as mask, the number of accessible stacks beneath a contact was controlled.

By vertically stacking InAs QDs on top of each other, separated by thin InP layers, triple barrier systems were realized [12,13,16]. One important feature observed is that the dots increase in size with additional layers. This means that the electron state energies for electrons in the upper dot are lower in energy as compared to in the lower dot. The small size shift is a feature critical for resonant tunneling to occur through the ground states of the dots in the structure, as it makes alignment of the ground-state energies at a certain applied positive bias possible. For tunneling to occur through a triple barrier system, it is required that the emitter states, and the electron states for the two dots align up resonantly at the same time as collector states are available. This results in very sharp current peaks, as was predicted by theory [17], and was observed experimentally [13].

The electronic states in InAs/InP dots have been characterized by optical investigations [18-20], and they have been calculated theoretically in the 8 band ***K•P*** model [21]. Size dependent electron state energies for the InAs/InP dot system were calculated by Holm *et al.* [22].

1.3.2 Structure proposed

In order to use the quantum dots stacks in applications, it would be beneficial to control the position of the device. By the creation of an artificial pattern, the position of the quantum dots can be pre-defined. In figure 4, the structure we have been working towards is presented. Unfortunately, up till now, no resonant tunneling through this type of structure has been observed.

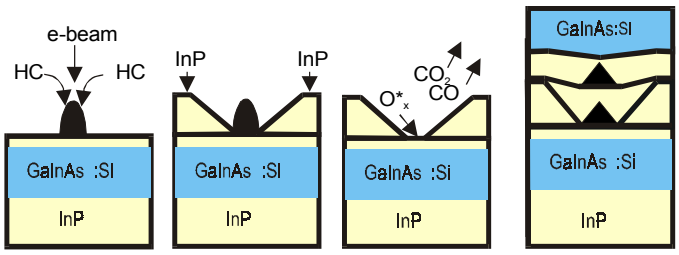

Fig 4 Schematics of the processing steps to spatially control where the self-assembled quantum dot resonant tunneling diode will form. Electron beam induced carbon deposits are used as growth masks. After partial overgrowth and removal of the carbon masks, dots preferentially nucleate in the holes at the surface. The final structure, on the right hand in the schematics, has the same band diagram profile as the structure with randomly distributed dots through which resonant tunneling was observed [12,13,16], except that the potential barrier, surrounding the active structure, is thicker outside of the active region.

2 Epitaxy

2.1 Introduction

The ordered growth of single crystalline material on top of a substrate is called epitaxy, which is a very important process in semiconductor technology. Some of the most common epitaxial techniques are liquid phase epitaxy (LPE) [2], hydride vapor phase epitaxy (HVPE) [23], metal organic vapor phase epitaxy (MOVPE) [24], ultra high vacuum chemical vapor deposition (UHV-CVD) [25], chemical beam epitaxy CBE [26], and molecular beam epitaxy (MBE) [27].

Epitaxy is a non-equilibrium process where the driving force is proportional to the supersaturation, σ, which causes a transfer of material towards, and incorporation of material into the crystalline phase. In a very simplified form the equation for the flux J of material is given by:

$$J=k\sigma$$

where k is the mass transport coefficient. The thermodynamic expression for the driving force, σ, can be written as a difference of the chemical potential of the component i in the mobile phase, liquid or vapor, and the solid phase, crystal:

$$\mu_i=(\partial G/\partial n_i)_{p,T,..} \qquad \Delta\mu\approx RTln(c/c_{eq}) \qquad or \approx RT\ ln(p/p_{eq})$$

where c and p are the actual concentration or pressure, respectively, of component i in the mobile phase, and c_{eq} and p_{eq} are the corresponding equilibrium concentration or equilibrium pressure of the component i in the mobile phase that is in contact with the solid phase. In addition to transfer of material towards the surface of the crystal, kinetically activated surface reactions can limit the growth rate. Finally, a too high growth rate can result in a poor crystalline quality.

2.2 CVD

A chemical vapor deposition (CVD) equipment can schematically be divided into different sub-units. For an accurate supply of precursors it contains a sophisticated gas delivery system, including precursors together with a distribution system for the carrier gas. Ultra-pure hydrogen, H_2, or ultra-pure nitrogen, N_2, can be used as carrier gas. The precursors are individually fed into a mixing chamber before they enter the reactor cell, which is designed in order to achieve a laminar gas flow above the substrate. The reactor is either cold wall or hot wall.

In a cold wall reactor, only the substrate is heated, typical for MOVPE conditions where the chemical reactions are endothermic. In a hot wall reactor, both the substrate and the gas phase are heated, which is typical for HVPE conditions where the chemical reactions are exothermic. In our case, (MOVPE, cold wall) the substrate is lying on a graphite susceptor that is heated by a radio frequency coil located outside the reactor chamber. The temperature profile obtained by heating the susceptor defines where material will be deposited, as reactions take place only at the hot parts of the reactor cell. Rest products, or molecules that pass the reactor without taking part in the growth process, are transported away via the exhaust system. The waste and excess gases are then burned. Alternatives to the burner are scrubbers or filters.

The most important processes during growth have been summarized by Stringfellow [28] and are listed below.

(i) Mass transport: the carrier gas carries the reactants to the reactor cell. A concentration gradient layer (boundary layer) [28] above the growing surface is formed by the laminar flow of the vapor in the reactor cell. Molecules have to diffuse through the concentration gradient layer towards the surface before surface reactions can take place. The growth pressure and the velocity of the carrier gas define the thickness of the concentration gradient layer.

(ii) Chemical reactions: must be taken into account for a more detailed description of the growth process. For instance, for MOVPE, some of the most important chemical processes for growth of GaAs, can be found in the handbook of crystal growth [29]. These are only a fraction of all involved reactions, as the chemistry is very complex. However, the net reaction follows as given by equation 1.

(iii) Thermodynamics: the growth rate is affected by thermodynamic properties since these define the deviation from equilibrium and thus the driving force for growth. The incorporation of native defects is influenced by thermodynamics. Furthermore, the reason to selective growth can be explained by thermodynamics.

(iv) Physical processes: adsorption of molecules and radicals at the substrate surface, heterogeneous deposition of molecules and radicals at the surface, surface diffusion of species at the surface, incorporation of atoms into appropriate lattice positions at kinks or steps, or desorption of reaction products that enter into the vapor phase and then are transported away by the carrier gas are other significant processes for the growth mechanism.

2.2.1 UHV-CVD

Ultra high vacuum chemical vapor deposition was developed in the late 1980´s [30] in order to make feasible the low temperature growth of Si and SiGe alloys. The benefits of a low temperature (500-600 °C) are increased interface abruptness, reduced solid state diffusion of dopants, and suppressed three-dimensional growth [31], as compared to traditionally CVD grown Si at atmospheric pressure at around 1100 °C by the use of $SiCl_4$.

Our UHV-CVD system uses a hot-wall reactor, and is a multiple-wafer system. The wafers are placed on a quartz boat, which is loaded into a quartz reaction tube heated by a conventional resistance furnace. For epitaxial growth, silane, SiH_4, and germane, GeH_4, are used as material sources.

In order to maintain the purity of the reactor, UHV sealing and continuous pumping are used, and the wafers are inserted through a load lock. UHV-CVD uses high vacuum (base pressure of about 10^{-9} mbar), and a low growth pressure in the range of 10^{-4} to 10^{-3}mbar, which guarantees low oxygen content in the layers grown [31]. Due to the extremely low pressure in the UHV-CVD chamber, the molecules are transported towards the surface essentially without colliding with each other. A direct impingement of molecules on the surface rather than a diffusive transport through a boundary layer is the responsible transport mechanism for source molecules towards the substrate. Gas phase reactions are suppressed; instead the growth is limited by surface reactions. The molecular flow between the wafers and the low sticking coefficients of silane and germane give the same flow on all the wafers, and make multiple wafer growth possible.

In our case, before UHV-CVD growth, HF is used to passivate the Si surface, protecting it from contamination while being loaded into the system, and ensuring a clean growth interface.

2.2.2 MOVPE

MOVPE was invented in the late 60s [32], and it has been named after the metal-organic compounds that are used as precursors for the metallic group-III elements. The metal-organic compounds are mixed with precursors containing a group-V element. When a supersaturated mixture of, *e.g.*, tri-methyl gallium, $Ga(CH_3)_3$, and arsine, AsH_3, is introduced above a heated GaAs substrate, an epitaxial film of GaAs can grow according to the following reaction:

$$Ga(CH_3)_3\,(g) + AsH_3\,(g) \rightarrow GaAs\,(s) + 3CH_4\,(g) \qquad \textit{(eq. 1)}$$

with the formation of methane, CH_4, as rest product, which can cause a background doping of carbon in the material, depending on V/III ratio and temperature. Other common precursors are trimethylindium, $In(CH_3)_3$, and phosphine, PH_3, allowing the growth of InP. Alloyed III-V compounds like, *e.g.*, $Ga_xIn_{1-x}As$ and $Ga_xIn_{1-x}P$ can also be grown.

The MOVPE process is complex, and the experimentally obtained results in MOVPE depend on the reactor configuration, the material to be grown, growth rate, growth pressure, and substrate temperature.

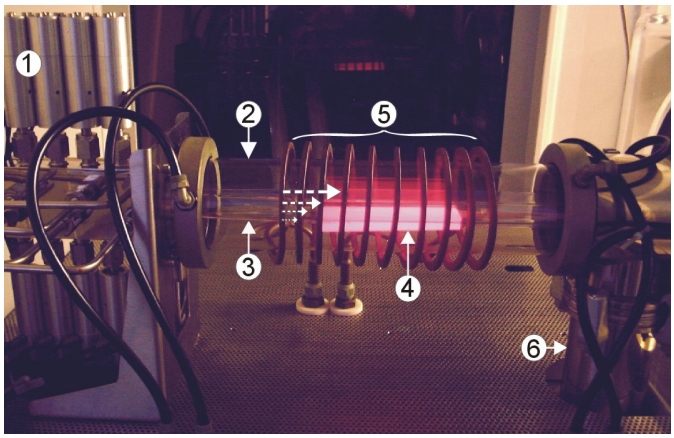

Fig. 5 MOVPE reactor, 1) Valve manifold to control mixture of gas entering the reactor 2) Outer cell 3) Liner (inner cell) through which the active reactants are passing 4) Graphite susceptor on which the sample is located during growth. It appears to be glowing because of black body radiation as the image was taken during heating of the susceptor. 5) RF generator coil. 6) Outlet. In the middle of the image, close to the susceptor, arrows indicate the flow direction. The length of the arrows indicates the shape of the velocity profile formed by the laminar gas flow.

2.3 Growth modes

When depositing hetero-epitaxial layers, there is a relatively limited amount of materials combinations that can be grown with closely lattice matched parameters. By combining lattice-mismatched layers, the range of available materials combinations may be increased, at the cost of incorporating strain into the materials grown. Depending on the amount of strain, the growth can lead to different surface morphologies. Three main growth modes can be identified [33].

(i) Frank Van-der-Merwe growth mode [34] is the situation when a layer grows in a pure 2D layer-by-layer manner. When the sum of the surface free

energy, γ_s, for the epitaxial layer and the interface free energy, $\gamma_{s/f}$, is lower than the free energy of the substrate surface, γ_f, it is energetically favorable for the epitaxial layer to completely cover the surface. In this case:

$$\gamma_s + \gamma_{s/f} < \gamma_f$$

If the epitaxial layer is lattice mismatched as compared to the substrate, the 2D growth can still continue, since a certain amount of strain can always be accommodated in the epitaxial layer. The epi-layer then deforms elastically, and the in-plane lattice constant of the epi-layer is forced to take the same value as the lattice constant for the substrate. Layers under compressive strain ($(a_{sub}-a_{epi})/a_{epi}<0$) expand in the growth direction, while layers under tensile strain ($(a_{sub}-a_{epi})/a_{epi}>0$) shrink in the growth direction. The accumulated strain energy increases linearly with the thickness of the deposited layer, and at a certain critical thickness of the epi-layer, it cannot accommodate more strain elastically: the epi-layer has to find other ways of relieving the strain.

One such way of relaxation is the formation of interfacial misfit dislocations, resulting in plastic deformation, which lets the epitaxial layer relax towards its free lattice parameter. This is common for thick layers with a small misfit.

(ii) For higher misfits, one way of relaxation is the second fundamental growth mode, represented by the Stranski-Krastanow growth [35], where the sum of the surface free energy and the interface free energy is about the same as the substrate free energy. The lattice mismatch in this case is commonly a few percent compressively strained. A layer, which is grown in a 2D fashion, undergoes a phase transition towards 3D growth as the accommodation of elastic strain in a pseudomorphic layer changes the balance between the surface and interface free energies during growth. This results in the formation of coherent (dislocation free) islands on top of a thin wetting layer:

$$\gamma_s + \gamma_{s/f} \approx \gamma_f$$

Note, as a curiosity, that in the original publication by Stranski and Krastanow, no strain effects were considered [35].

Fig. 6 Schematics of the three fundamental growth modes in hetero epitaxy. From the left: Frank Van der Merve growth mode, Stranski-Krastanow growth mode and Volmer-Weber growth mode

(iii) In the case when the surface free energy of the epitaxial layer plus the interface free energy is larger than the substrate surface free energy, it is energetically more favorable to have the substrate surface exposed to the vapor, as compared to the epitaxial layer. This leads to the formation of 3D clusters on the surface, called Volmer-Weber growth [36], usually observed for strained layers with a lattice mismatch >10%:

$$\gamma_s + \gamma_{s/f} > \gamma_f$$

2.4 Self-assembled island formation

The first observation of self-assembled island formation, which is a special case of the Stranski-Krastanow growth, was made in 1985 [37]. During epitaxy, the deposition of the island material starts with a complete wetting of the substrate. As the deposition continues, the accumulated strain energy, E_{el}, increases linearly with the wetting layer thickness, according to $E_{el}=c\varepsilon^2 t$, where c is the elastic modulus, ε is the lattice mismatch, and t is the wetting layer thickness. The deposition rate, R,

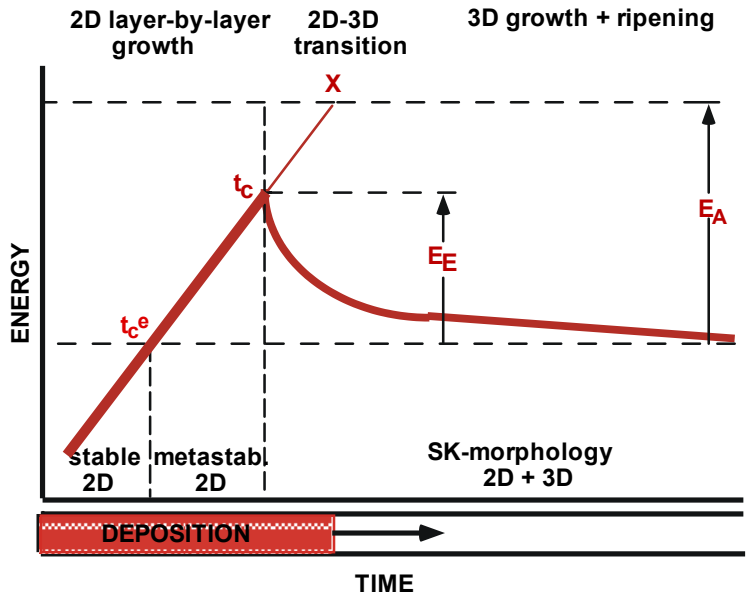

Fig. 7 Schematic of the total energy vs. time for the self-assembling process. t_c^e, and t_c are the thermodynamically and kinetically defined critical wetting layer thickness, E_E is the excess energy due to strain, and E_A the 2D-3D activation barrier. X is the point where a pure strain-induced transition becomes possible (no thermal activation) [38].

is constant and therefore E_{el} , and consequently the total energy of the system, increases linearly in time, see figure 7.

When the wetting layer thickness exceeds the equilibrium wetting layer thickness, t^e_c in figure 5, the system enters a meta-stable region. There is potential for island formation, but the activation energy for the formation needs to be overcome. When the critical wetting layer thickness, t_c is reached, the island nucleation starts and the wetting layer starts to decompose. Mobile adatoms from the decomposing wetting layer stick together with the deposited adatoms at the surface, and island nuclei form. When these nuclei become larger than a certain critical size, determined by surface and interface energies and bond strength, they grow steadily. Before the nuclei reach this critical size, they run the risk to dissolve [39].

Examples of some suitable materials combinations for island growth are, for instance, InP on $Ga_xIn_{1-x}P$/GaAs, $Ga_xIn_{1-x}As$ on GaAs, $Ga_xIn_{1-x}P$ on GaP, InAs on InP, and Ge_xSi_{1-x} on Si, amongst others.

2.4.1 Dot size, homogeneity, and density

Vast research has been done in the field of quantum dot formation. For device applications, requirements of homogeneity, size-control and site-control of the dots have been, and are, challenging tasks.

It has been shown that the density and size of coherent islands primarily vary with the deposition temperature and deposition rate [40-44]. The characteristic length scale of nucleation in nucleation processes is usually written as $L \propto (D/R)^{\gamma}$ [45]. $D(T)$ is the temperature dependent diffusion constant, $D(T)=D_0 \times exp(-E_d/kT)$, where k is Bolzmann´s constant, T the absolute temperature, and E_d the energy barrier for surface diffusion. D_0 depends on the specific surface. The exponent γ is determined by the actual process. For self-assembled island growth, Johansson *et al.* [44] found γ to be about ½. By using half the observed island separation as L, $L=1/(2\rho^{1/2})$, with ρ being the density of islands, the density ρ was expressed as a function of R/D, $\rho \propto R/D$ [44].

In other words, the density of dots increases with increasing deposition rate (super-saturation), while it decreases with increasing temperature. Note that the deposited material is distributed over the stable growing nuclei, thus one can expect an increase in size of the dots with decreasing density [38].

Another way of affecting the sizes of the dots, which can increase the size homogeneity of the dots, is to insert an annealing step after deposition of the dot

material [46]. For longer annealing periods, the size of the dots decreases as material moves from the dots to the wetting layer.

A common tool for measuring densities and sizes of self-assembled islands is atomic force microscopy. To get further information on the homogeneity of the dots, photoluminescence is often used, the narrower the emission linewidth the better the homogeneity and the more suitable for applications, like lasers for instance. For an overview of the field of quantum dot lasers, Grundmann's review article can be recommended [47].

2.4.2 Interface reactions

For growth of any heterostructure, the quality of the interfaces is very important. Interface reactions and materials intermixing will ultimately determine, for instance, the quality of a grown quantum well. Therefore, the exchange between arsenic and phosphorous atoms on InP has been widely studied [48-55].

Like expected for a chemical reaction, the As-P exchange reaction depend on the specific conditions, like for instance, temperature, pressure, and time, $f(t,T,p...)$. It was found that the process had an activation energy of about 1.23 eV on (001) InP [52], and that it was reversible [51,52].

In studies of MOVPE grown GaInAs/InP quantum wells, Seifert *et al.* [53,54] observed As-P exchange reactions at the InP/GaInAs interface, as well as a concentration gradient of As in the following InP, starting with the GaInAs/InP interface. At the lower interface, P with its higher vapor pressure is easily desorbed and replaced by As atoms. At the upper interface, the As concentration gradient is observed due to As carry over effects [53,54].

The carry-over was suggested to originate in arsenic deposition at the susceptor and the walls of the inner cell to the reactor, in combination with excess As adsorbed on the surface working as a source for carry-over. A correlation between the growth conditions that determine the surface reconstruction of the material was observed [53,54]. High AsH_3 pressure and low temperatures favor the formation of excess As adsorption layers, which are an efficient source for As carry-over.

For strain driven island growth, the exchange reaction significantly alters the kinetic processes of the QD formation [18,56,57]. In the extreme case, InAs dots on InP were produced by annealing of InP at 600 °C under As containing ambient, and then cooling down [58].

Due to carry-over effects [53], more material for dot formation becomes available when capping InAs QDs with InP, as the already cracked AsH_3 reacts

with the incoming material. In our case, in order to reduce such carry over effects we use a switching sequence where first the group III is switched off, then after a delay time of one second, the group V precursors are switched, and then after another second delay time when the surface is annealed under the appropriate group V gas, the group III material is sent to the run line.

Poole *et al.* [59] recently demonstrated that at a growth rate of 2.68 Å/s, the luminescence from InAs/InP dots was observed at about 1.6 μm, whereas when capped with a growth rate of 0.43 Å/s, the dot luminescence was shifted to a wavelength of about 1.4 μm. The authors interpreted this as a reduction in size of the dots during the capping procedure, as In atoms migrate off the QDs to incorporate preferentially on the wetting layer, during the time given for the reverse reaction to occur at lower growth rates.

Furthermore, strain and patterning of the surface can induce enhanced exchange reactions, and possibly, enhanced material transport to regions with larger lattice constant or to areas with surface curvature. Experimentally, locally enhanced As-P exchange reactions were used for site-selective InAs/InP QD growth [60,61]. In fact, dots have been grown in patterns at normal InAs QD growth temperatures (about 500 °C, MOVPE) without any InAs deposition, the dots formed by As-P exchange reactions only [62].

Regarding the composition of dots formed by the use of As-P exchange reactions, it has been a general belief in literature that those consist mainly of pure InAs, rather than being significantly alloyed $InAs_xP_{1-x}$. We recently studied InAs quantum dots that were formed partly by As-P exchange reactions, by cross sectional scanning tunneling electron microscopy [63], and we confirmed that these dots were mainly pure InAs.

In addition to pure exchange reactions, materials intermixing has been observed in several materials systems, like for instance in Ge dots on Si, which usually contain some Si [64,65], and for InAs on GaAs that usually consist of $Ga_xIn_{1-x}As$ [66-68]. One major difference between growth of InAs in InP, and InAs/GaAs, is that it is the group V species that changes between the QD and the barrier material for InAs/InP, not the group III as for InAs/GaAs.

2.5 Vapor-liquid-solid growth

The growth of needle shaped crystals has been known for centuries. In the 1960´s, Wagner and Ellis proposed an explanation for such whisker growth, referred to as vapor-liquid-solid (VLS) growth [69,70]. The VLS mechanism is in principle a variant of the ordinary liquid phase epitaxy.

Liquid phase epitaxy is based on the interaction between a melt and a solid phase. For growth of GaAs, for instance, the melt usually consists of liquid Ga containing dissolved As. At a certain temperature, Ga and As are in equilibrium according to the phase diagram of GaAs [24]. By lowering the temperature of the solution, the liquid becomes undercooled and GaAs precipitates on the solid surface. The phase transition is close to equilibrium and the growth rate is limited by diffusion through the melt.

In the case of VLS growth, a metal particle is located on the surface forming a liquid/solid interface, thus forming a local LPE system. So far, for the growth of Si or III-V whiskers, Au has predominantly been used as catalyzing metal particle, even though a number of other metals can be used [70]. For VLS growth, the super-saturation required for growth is obtained by an inflow of material from the vapor and adsorbed species diffusing on the surface. In figure 8, the schematics of VLS growth according to Wagner [70] is presented.

The growth of nanometer-sized whiskers is interesting from more than one aspect. Firstly, from a structural point of view they could be used as scanning probes [71], or as field emission tips [72]. Then, all classical experiments in semiconductor physics, using pn-junctions, could be remade with this new way of creating quantum based electronic devices.

In MOVPE, the proper conditions for whisker growth in the VLS growth mode can be met, and in the 1990´s Hiruma *et al.* [73] made some pioneering work

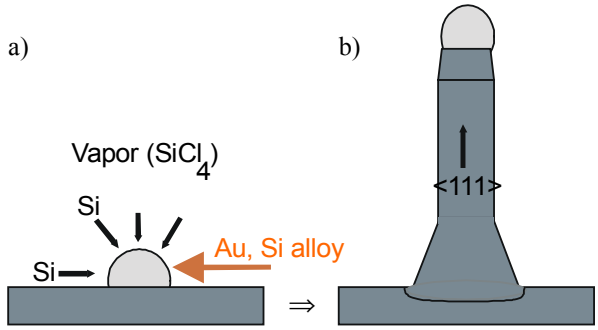

Fig. 8 Schematics of VLS growth of Si whiskers [69]. a) Commencing growth. Si, deriving from $SiCl_4$ in the vapor and Si adsorbed on the surface, diffuses to the Au particle where it enters to form an Au/Si alloy. When the Au is super-saturated with Si, a wire will grow in the <111> direction as Si precipitates at the AuSi/Si interface. b) After growth, the narrowing of the whisker at the top illustrates the change in Si/Au size due to Si depletion of the alloy after switching off the precursors and then cooling down. At the bottom of the whisker, tapering is illustrated, which is material that deposits at the side of the whisker.

on wire growth. The authors evaporated thin Au films on the substrates. By varying the thickness of the films deposited, differently sized Au particles (nano-scale) could be achieved by annealing the samples at appropriate temperature. Electrical and optical characteristics of nano-whiskers, including hetero-structures were studied [73-76]. It was found that the preferential direction for whisker growth was the <111>B direction. Recently, other directions for whisker growth in the VLS growth mode have been observed, like <112> and <110> [77]. By VLS growth of GaAs nano-whiskers in MOVPE [78], it was shown, that it is not the reaction at the (-1-1-1)B/(Au,Ga)-interface which limits the whisker growth rate, but the processes outside the Au droplet, *i.e.*, the Au droplet did not affect the activation energy of the global deposition process.

Lately, whisker growth research has gained new momentum. Ohlsson *et al.* [79] used size-selected Au particles [80] to control the diameter of the whiskers. For whisker growth in the VLS growth mode, the growth position is determined by the position of the catalytic metal particle, and site-controlled whisker growth was realized by the use of masking and gold deposition [81]. Recently, by the use of electron beam lithography and lift off, InP whiskers were grown in predefined arrays [82]. Another way of controlling the sites for whiskers has been to situate Au particles, by the use of atomic force microscope, in desired positions [79,83].

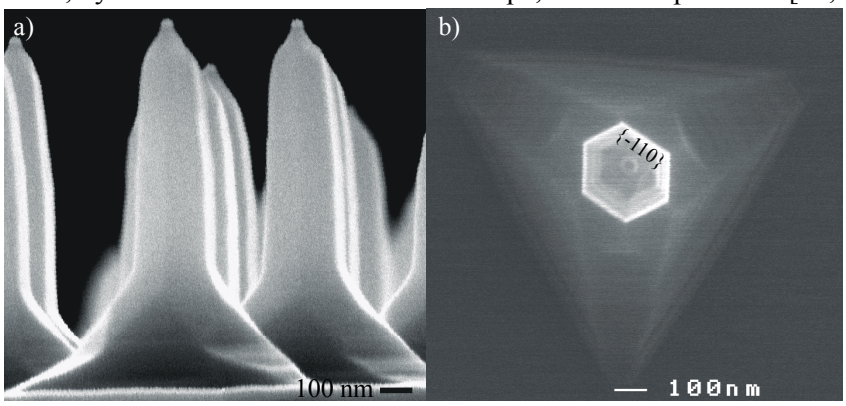

Fig. 9 Scanning electron microscope images of core shell structures. a) Side view. b) top view. GaAs whiskers were grown from 40 nm diameter Au particles, and then the GaAs nano whiskers were radially capped by AlGaAs deposition. The Au particle can be seen at the top of the whiskers. The pronounced base of the whisker formed during the capping procedure. The whisker side facets are {-110}, as indicated in figure b). At the base, facets with decreasing steepness the further away from the center of the whisker form, as confirmed by AFM.

In addition to VLS growth on an epitaxial substrate, other methods for producing nano-wires have emerged, like for instance, laser ablation [84] and thermal evaporation of solid sources [85].

Nanowires have been grown in several materials systems, using group IV, [86,87] group III-V, [73,88-90] and group II-VI elements [77,91], including structures with variable composition and doping, such as InAs/InP [89], GaAs/GaP [92], Si/SiGe [87], and *n*-type/*p*-type InP [92]. The fabrication of one-dimensional hetero-structures was reported by several groups [89,92-94], and their functionality in resonant tunneling structures was demonstrated, using an InAs/InP material combination [95]. Single electron transistor (SET) [96] characteristics were observed in such wires, by the use of high-resistive contacts that resulted in an island coupled to the electrodes via tunnel barriers [97], and by the use of an InAs island embedded in InP tunnel barriers [98]. Gudiksen *et al.* [92] demonstrated light emission from segments of GaAs embedded in GaP, which has a larger band gap. In the same paper the authors also demonstrated InP LEDs.

3 Site control

3.1 Introduction

So far, the discussion has been kept on randomly distributed QDs and nano wires. For the realization of many applications, it would be desirable, or necessary, to control the position of such quantized objects. For instance: promising novel concepts like quantum cellular automata rely on assembling dots in close enough proximity to observe both tunneling and Coulomb coupling between them [99]. Another example is resonant tunneling diodes, which were suggested to be excellent candidates for the creation of digital circuits, because of high switching speed, low power consumption, and reduced complexity in implementing a given function [100]. Our quantum dot resonant tunneling diodes show impressive IV-characteristics, but are of little use for electronic circuits, for instance, when appearing randomly on the surface, though in a certain density.

For site-controlled QD growth, some further advantages have been predicted. The QD size distribution is expected to narrow by site-control, as has been suggested theoretically [101,102] and observed experimentally in multi layered dot structures [103]. It could also be feasible to manipulate the density and size of the QDs independently, in contrast to the normally observed behavior that the size is inversely dependent on the density of the dots due to materials balancing at the surface [104].

Furthermore, arrangement of low dimensional structures with nanometer precision in desired positions, laterally and vertically, would open the way to interesting fundamental physics studies. The site-control of semiconductor quantum dots, from a general point of view, can be explained by a combination of thermodynamics and kinetics.

3.2 Modification of the surface chemical potential

Variations in the chemical potential, μ, determine the driving force for epitaxy. Therefore, gradients in the chemical potential along the surface are expected to induce surface diffusion fluxes towards regions with lower μ, something that Herring [105] proposed already in 1950. In the same paper he discusses the dependence of the chemical potential, just beneath the surface of a thin film, on curvature and strain. The generally accepted formula for the chemical potential of

the component i of an alloy at a growth temperature T, originating from Herring, can be written as [106-110]:

$$\mu_i=(x,y,z=0)=\mu_0 + \gamma\Omega\kappa(x,y) + \Omega E_s(x,y)+ k_bT\, lnx_i(x,y) \qquad (eq.\ 2)$$

where μ_0 is the surface potential for an unstressed surface of the material. The second term is from the contribution of surface curvature, $\kappa(x,y)$, the third term comes from the local strain energy on the surface, $E_s(x,y)$, and the fourth term is a contribution due to mixing. Ω is the atomic volume, γ is the orientation dependent surface free energy, and x_i the component mole fraction.

For self-assembled quantum dot growth, as represented by the Stranski-Krastanow growth mode, the growth starts with a complete wetting of the substrate. In a first approximation, diffusion of material towards areas with lower chemical potential cause locally enhanced growth rates, with the effect that the critical wetting layer thickness for 2D-3D nucleation can be reached earlier locally.

In literature, examples of studies on pure surface curvature effects and pure strain related effects on the surface chemical potential can be found. For strain driven quantum dot growth, where the formation of 3D nuclei leads to strain relaxation, the local strain potential must always be taken into account, whereas surface curvature does not play a role for growth on planar surfaces. Lets initially separate the two for simplicity.

Regarding surface curvature effects, Biasiol *et al.* [109,112] studied epitaxial growth of AlGaAs on patterned GaAs surfaces. The authors observed Ga rich vertical channels at the bottom of the deeply etched grooves [109] after AlGaAs deposition. The authors used a one dimensional model to explain the self-

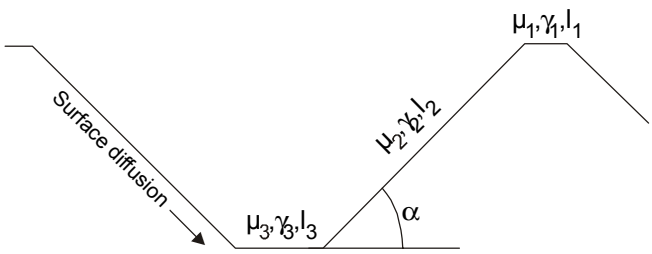

Fig. 10 A non-planar surface, as modelled by Ozdemir *et al.* [111]. l_i γ_i and μ_i denote the length, surface free energy, and the chemical potential of the facet i. $\gamma_1=\gamma_3$ since they have the same orientation. For this simplified structure, Biasiol *et al.* [112] calculated the surface chemical potential for the different facets in a one-dimensional model, and showed that the chemical potential of the facets were not thermodynamically equivalent due to curvature. They found: $\mu_1=\mu_0+\gamma\Omega_0/l_1$, $\mu_2=\mu_0$, $\mu_3=\mu_0-\gamma\Omega_0/l_3$, with μ_2 taken as μ_0, and $\gamma= 2(\gamma_2 \csc(\alpha) - \gamma_1 \cot(\alpha))$

limiting profile evolution of the AlGaAs layers observed in their experiments, taking into account growth rate anisotropy, curvature-induced capillarity, and for alloys, entropy of mixing, whereas strain related effects were considered to be negligible. Following Ozdemir *et al.* [109,111,112], the variations in surface chemical potential due to surface curvature were evaluated for a facet, bounded by N other facets (see figure 10 for an illustration). The results were explained by the stronger Ga diffusion with respect to Al [113] towards the bottom of the hole, the driving force being gradients in the local surface chemical potential.

Regarding the strain related part; due to the inherent strain of the dot material, locations favourable for dot nucleation are those that allow for efficient strain relaxation. Penev *et al.* [114] showed that the activation energy for surface diffusion of In on a GaAs surface was affected by surface strain, and calculated that with increasing tensile strain in the GaAs, it was easier to nucleate an InAs island in the tensile strained region. The effect of patterning is more complex than merely adding surface curvature. Patterning may give rise to areas that are efficient for strain relaxation. Dots have, for instance, been observed at edges of mesas [115], and the top corners of pits [116]. Another effect of patterning that can occur as a result of anisotropic growth rates on the facets exposed, is surface strain induced by phase segregation of a material. For instance, a ternary deposited on a patterned surface can be inhomogeneous in its materials composition due to mass transfer of species with higher mobility on the surface to faster growing facets.

A commonly observed phenomenon, discussed in chapter 3.5, is the vertical alignment of successive dot layers, separated by thin spacer layers. A buried material under strain can create a strain field on the growing surface. Theoretical calculations on the resulting strain field due to buried islands have been performed, focusing on the nucleation event [117] or on strain induced surface diffusion due to lowered local chemical potential [108,118] for various materials systems, like III/V [108], II/VI [110,118,119], IV/VI [110,118] and IV [110,118]. Commonly, continuum elasticity theory has been used for such calculations, and it was shown that outside of the highly strained islands, these were in good agreement with atomistic elasticity calculations [120].

3.3 *In-situ* spontaneously ordered dot growth

The spontaneous ordering of self-assembled dots along naturally available surface steps has been observed for InAs/GaAs [121], as well for InAs/InP [122]. By growth on vicinal surfaces, step bunching can be used to amplify this effect, which

was intentionally done by Kitamura *et al.* [123] on samples with a miscut of 2° (InGaAs/GaAs, 500 °C, MOVPE).

For high-density systems, the individual quantum dots are not elastically independent from each other. Moison *et al.* [124] noticed a tendency to form hexagonal arrangements of InAs/GaAs, at dot densities of 4×10^{10} cm^{-2}, that improved in periodicity with surface flatness (500 °C, MBE). At even higher densities, of about 10^{11} cm^{-2}, Ruvimov *et al.* [125] observed islands with a tendency to form a primitive two-dimensional square lattice (InAs/GaAs, 480 °C, MBE). The authors suggested that temperature and strain (kinetics and energetics) would be important factors for spontaneous ordering of dots. The lateral ordering by use of inhomogeneously strained surfaces was shown by Xie *et al.* [126] who formed arrays of Ge islands on relaxed Si templates by the use of an underlying dislocation network. Mano *et al.* [127] used strained superlattices to align InAs dots on underlying wire-like structures in GaAs.

Lately, quantum dots that align vertically on top of each other, due to surface strain created by lower lying dots has received a lot of attention, which will be discussed separately in section 3.5.

3.4 Lateral positioning of dots by surface patterning

Site-control of QDs by modification of the surface before dot formation has been realized by several groups and by several means.

Complete *in-situ* methods ought to be the most feasible. Recently Schmidt *et al.* [128] reported on the complete *in-situ* growth of ordered InAs/GaAs QD bi-molecules. A single layer of InAs quantum dots (500 °C, MBE) was partially overgrown with 10-nm-thick GaAs. *In-situ* etching in $AsBr_3$ was then used to preferentially etch away the material disturbed by underlying quantum dots, and holes with diameters of 40–60 nm, elongated in the <110> direction were developed at the surface. When InAs was deposited onto this surface, the reported [128] QD bi-molecules formed at the surface. These dots were then used as seed dots for stacking, and the authors [129] report on a PL-linewidth as narrow as 16.0 meV for a sample with twofold stacks, separated by 5 nm GaAs. This method is still “random” since the nucleation sites are defined by a first randomly deposited dot layer.

The following methods have the disadvantage that at least one stage of pre-patterning of the substrate needs to be performed. However, they benefit from better-defined starting conditions, and also make feasible the realization of special structures. Several authors have reported on pre-patterning of the surface in order

to position the islands. Artificially created mesas, trenches, and holes are commonly used. Ishikawa *et al.* [130] used *in-situ* electron beam lithography to define nucleation sites for InAs/GaAs islands (MBE, 460 °C), and also showed that the density of dots in a hole decreased with the depth of the hole. At a hole depth of 5 nm, local densities of 1×10^{11} cm^{-2} in the patterns were observed, after a deposition of 1.8 ML InAs on the patterned surface, a value which is close to the concentration limit for QDs with a width of 30 nm. When the hole was shallower than 1 nm, no dots were found in the holes.

One of the most common methods of controlling the island sites is a combination of *ex-situ* electron beam lithography and wet chemical etching to create trenches and holes at the surface in which the dots nucleate [131,132]. By such patterning, it was demonstrated that InAs/GaAs islands preferentially nucleate on B-type facets, and that they avoid A-type facets. Similar results were found in MBE [131] (InAs/GaAs), CBE [133] (InAs/GaAs), as well as MOVPE [38] (GaInAs/GaAs). It was argued that the effect could be explained by different surface mobility of In adatom on A and B facets. In addition to anisotropic growth rates, surface reconstruction, and preferential intermixing of materials may

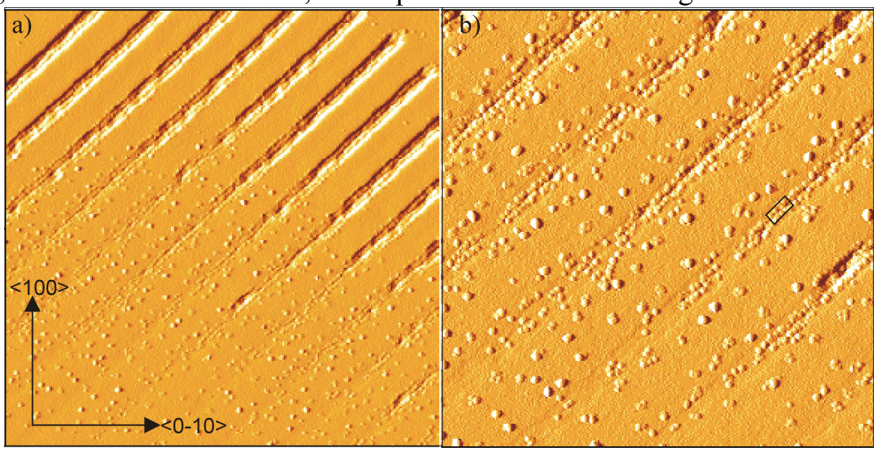

Fig. 11 InAs/InP QDs deposited on trenches fabricated by electron beam lithography and wet chemical etching. a) Non-homogeneous trench depth can be observed, 0-50 nm in depth. Around shallow or non-existent trenches, dots are observed on the planar surface, whereas when the trenches get more pronounced and deeper, no dots can be observed on the planar surface close to the trenches, instead the dots nucleate within the trenches. This indicates an increasing driving force for material diffusion towards, and incorporation at the trenches with increasing depth of the trench. 8×8 μm^2 AFM image. b) Zoom in that shows the dots in the trenches. The local density of dots in one trench, as indicated by the drawn square, is 3×10^{10} cm^{-2}. 4×4 μm^2 AFM image

contribute to the differences. Jeppesen *et al*. [133] measured the luminescence of the wetting layer, observing a shift in emission energy from the different facets on the patterned surface, thus showing that the wetting layer thickness varied on different facets.

Under our conditions (MOVPE; 500 °C) the InAs/InP system does not show the same preferential dot nucleation on B-type facets as that observed for the GaInAs/GaAs system [38]. We deposited 0.9 ML InAs on (001) InP surfaces, patterned by carbon nano-growth masks, which were partially overgrown and then removed by oxygen plasma etching. The results can bee seen in figure 12.

One may argue that one of the differences between the GaInAs/GaAs and InAs/InP system is the As-P exchange reaction present in the InAs/InP system. Kappelt *et al.* [134] found that As/P exchange is a facet sensitive process, with the most aggressive reaction on (111)B, the least on (001), and (111)A intermediate. It is however, not yet clear why the InAs/GaAs islands prefer the B-type facets, nor why the materials systems differ, and the arguments remain speculative.

Lefebvre *et al.* [61] reported on the growth of InAs QDs on oriented InP mesas, each with a top (001) InP facet, grown in etched SiO_2 windows (CBE, 500 °C). Interestingly, when comparing dot formation on the different mesas, large InAs clusters were found on the top (001) facet for <110> oriented stripes, whereas almost no islands were observed on the (001) surface for mesas oriented in <100> and <-110>, with (110) and (111)A side facets respectively. The results were discussed in terms of inter-facet mass transfer of exchanged material from (111)B to the (001) plane, but less efficient exchange reactions and lower In surface mobility on (111)A and (110). The authors showed that the dots aligned on top of

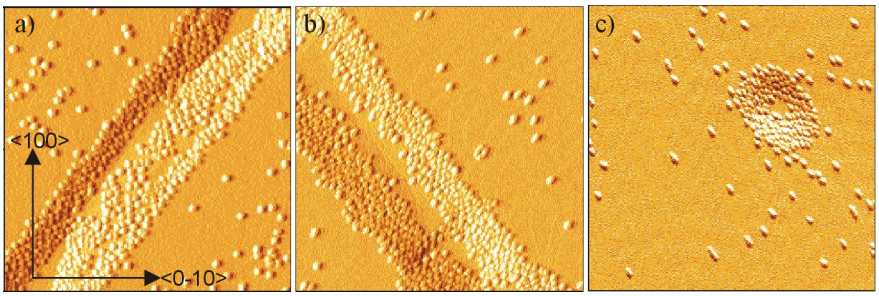

Fig 12 InAs/InP islands formed by 0.9 ML InAs deposition on a patterned surface at 500 °C. a) Trench in <1-10>, b) trench in <110>, c) hole. The patterns were created by partial overgrowth, and then removal, of electron beam induced carbon growth masks [60]. It is visible that the dots have no preference between A-type or B-type facets, in contradiction to previous observations in the GaInAs/GaAs system [38]. 2×2 μm^2 AFM images.

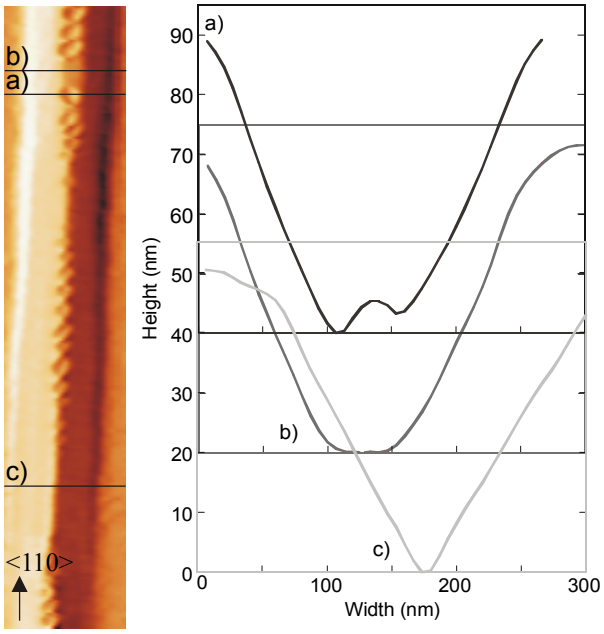

Fig. 13 Selective dot nucleation of InAs/InP in a 50 nm deep trench formed by lithography and wet chemical etching. Non-uniform dot nucleation in the trench can be observed, a-c) line scans, as indicated in the AFM image to the left, which indicate the surface profile. Dots form in the intersection between the B-type facet and the (001) plane in the bottom. Note that the dots observed seem larger in size when the (001) plane that develops in the trench is wide, but smaller when the extension of the plane is narrower. At a width of the bottom plane of about 40 nm the dots are fully developed.

the mesas, and that the luminescence from these dots was tunable in an energy range as wide as 0.84 eV to 1 eV, by varying the width on the top mesa [135].

For non-polar materials, like SiGe/Si, no polarity-induced effects are expected. For such materials, selectivity and inter-facet diffusion can occur due to growth rate anisotropies [136]. Kamins *et al.* [137] deposited Ge dots selectively on Si mesas in etched SiO_2 windows, aligned in <110> and <100> directions. Dots were observed to align preferentially on the top (001) plane of mesas oriented in <100>. Jin *et al.* [115,138] observed Ge dots at the edges of top (001) planes on Si mesas in etched SiO_2 windows. The results when using such mesa structures was discussed in terms of efficient strain relaxation at the edges of the mesas [115,137,138], and mass transfer from the sidewalls of the Si mesas.

One important aspect when using a large area growth mask for selective growth in etched windows is that the mask is growth inhibiting. Especially for

CVD processes, this results in a higher super-saturation next to the mesa, and mass transfer toward the mesas and the growing facets.

For growth of Ge islands on etched mesas in Si without the use of any growth mask, Zongh *et al.* [139] observed Ge islands in trenches between the Si mesas, indicating the diffusion of material downwards from the top terrace to the bottom of the mesa. The conditions before dot growth where then changed by the deposition of a strained SiGe super-lattice before island growth on the mesas, thus introducing an anisotropic strain field at the surface. In contrast to nucleating in the trenches between the mesas, the dots were then observed at the top of the (001) mesas.

Obviously, temperature is a very important parameter that affects the kinetics in the system. For instance, Jin *et al.* [138] found only one dot on Si mesas, when grown at 700 °C, whereas four dots were observed at a growth temperature of 600 °C. By increasing the temperature, two major effects are expected for the Ge/Si system; i) increasing surface mobility and mass transfer to the faster growing facet, ii) stronger intermixing of Si into Ge [65], reducing the lattice misfit and increasing the base width of the islands. Zhong *et al.* [140] observed selective dot growth at the bottom of etched trenches, between mesas, at 650 °C, whereas at 600 °C the nucleation was less selective. The authors explained their results in a kinetic model, where the flux of material downwards the mesa was motivated by a smaller activation barrier for diffusion downward a step than upwards.

Recently, alternate methods for positioning with high position control, in the nanometer range, were presented. Kohmoto *et al.* [141] used STM induced deposits for patterning of a GaAs surface, and after GaAs overgrowth of the deposits without planarising the surface, InAs/GaAs QDs (460 °C, MBE) were site selectively grown in the patterns by deposition of about 1.1 ML InAs. This amount of material is less than the critical wetting layer thickness for InAs/GaAs, which was reported to be about 1.5 ML [121], indicating the selective diffusion of material towards the pits at the surface. We used electron beam induced deposits for patterning of the semiconductor surface to align single InAs/InP dots (MOVPE) [60], or quadruples of Ge dots in pits (UHV-CVD) [116].

By deposition of Ge on Si, dot quadruples were found in randomly distributed holes over the surface, formed by deposition of Si and C on the initial Si(001) surface under MBE (650 °C) conditions [142], as well as by varying the deposition rate in MBE (550 °C) [143]. We used electron beam induced carbon pre-patterning to arrange such quadruples in an ordered fashion under UHV-CVD (620 °C) conditions. By Si growth on the pre-patterned surface, faceted pits form at

each deposit. Dots nucleating on this surface were observed at the intersection between the facets, and the results were discussed in terms of the local surface chemical potential [116]. Dots were seldom observed in the bottom of these holes, probably due exposed carbon masks remaining in the bottom of the pits.

Up to now, surface curvature has been presented as a means to alter the chemical potential locally, where the directed diffusion of material due to the gradients in the chemical potential affect growth rates locally. In addition, surface curvature may affect the nucleation event. Thermodynamically, the nucleation work is the lowest on a concave substrate, it is greater on a flat surface, and it is the greatest on a convex surface [146]. Based on the condition of the critical nucleus formation, $d\Delta G/dr=0$, when the atomic cluster has equal probability to either grow or disappear spontaneously, the radius of the critical nucleus was found to depend on the angle between facets [147], *i.e.*, the atom number that the critical nucleus consists of is smaller in the hole as compared to the flat, and stable nuclei forms faster at concavely formed areas. It is commonly observed that dots nucleate at the

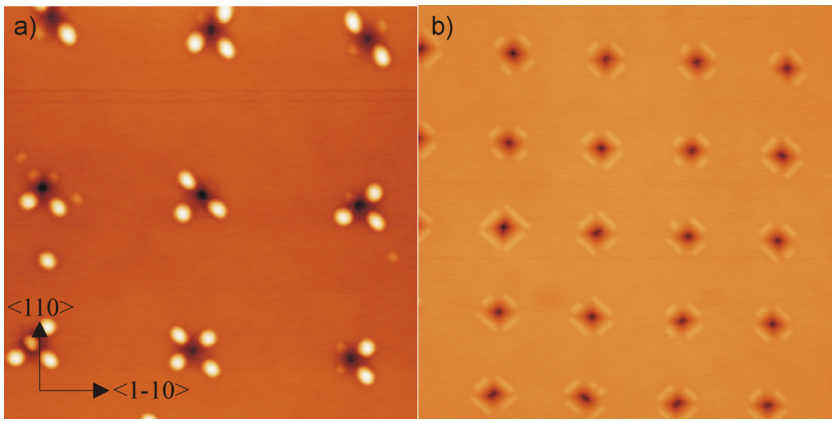

Fig 14 SiGe/Si islands grown on a patterned surface with pits. a) Pyramids and domes are observed in the patterns. At first, quadruples of pyramid-shaped Ge dots are formed that can grow with the supply of more Ge to become dome-shaped. This is in agreement with the understanding of the often observed 'shape transition' as a consequence of materials balancing at the surface [144,145]. Dots are positioned at the <110>/<1-10> intersection of the pit edges. Islands on mesas are generally observed as pyramids or domes [115,138,139]. b) Quadruples of laterally extended SiGe/Si islands are observed in the pits. The extension in the <100> direction is most probably due to the formation of strain relieving SiGe growing at the edge of the pits [142]. 2×2 μm^2 tapping mode AFM images

intersection between two facets inclined towards each other in a concave fashion [60,116,128,140].

3.4.1 Electron beam induced carbon deposition for patterning

When SEM is used to monitor microscopic structures, the surface being observed is inevitably contaminated. This is due to the fact that residual hydrocarbon molecules from the oil in the diffusion pump remain in the SEM chamber even at low base pressure (typically 10^{-5} Pa in our case) and are decomposed by irradiation of the electron-beam. Since this process occurs only on areas that are exposed by the electron beam, nanometer sized carbon contamination can be deposited on surfaces.

One use of these deposits has been to produce extremely sharp so-called super AFM-tips by focusing the electron beam on an ordinary AFM-tip [148]. Other ways to use these deposits have been as growth masks [60,149], and as etch masks [150]. The deposits have been used as the active part in the realization of a lateral resonant tunneling structure [151], where carbon deposits were arranged in series between metal electrodes to form the device. Recently, the carbon deposits were used to fabricate nano-sized tweezers [152]. In the current thesis the possibility of depositing carbon in SEM has been utilized to make nano-growth masks and AFM super tips.

The deposition rate of the carbon has been found to vary with acceleration voltage and probe current [153]. The diameter of the deposits will be defined by the spot size, which depends on the acceleration voltage, the beam current, and the focus. Long beam irradiation leads to vertical as well as lateral deposition, where backscattering of electrons from the substrate causes the lateral deposition. A high acceleration voltage leads to an increasing height/width ratio. The growth rate of the carbon is decreasing with the size of the deposit, most probably due to charging effects. The carbon is an insulating material, and will therefore be charged by the electron beam. Coulomb forces deteriorate the electron beam and hence deposition is suppressed. Another possible explanation is that, as the carbon pillar is growing longer, we move out of focus of the electron beam. The growth rate depends on the background pressure in the SEM and varies from system to system.

Since the deposits are mostly of carbon [154], they can be removed from the surface by oxygen plasma etching, before and after partial epitaxial overgrowth. The carbon deposits being exposed to the oxygen plasma react and form carbon monoxide and carbon dioxide. Therefore, oxygen plasma can be used to effectively remove the thin carbon deposits, induced by backscattering of

electrons at the surface [10], at the same time as the carbon growth mask is reduced in size by the treatment. The etching rate of the carbon increases with decreasing pressure in the plasma, whereas the etching rate after partial overgrowth of the carbon decreases somewhat, probably due to hydrogen desorption at the high growth temperature (630 °C).

Another way of using this deposition technique has been to insert metallic precursors into the SEM chamber to produce conductive carbon deposits [155].

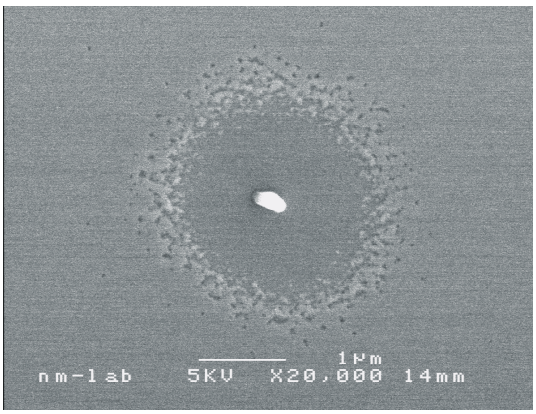

Fig. 15 Top view SEM image of carbon deposited for 20 s ∂ 100 pA (c.a. 1.5 μm in height), after which 50 nm GaAs was deposited. It is visible how growth is prohibited no only at the central deposit, but nearby the deposit as well. Scattered electrons cause a thin carbon film around the main deposit. The thin layer can be removed by oxygen plasma etching [60].

3.5 Vertical stacking of quantum dots

Already in 1985, Goldstein et al [37] observed that MBE grown InAs/GaAs islands aligned vertically, forming one-dimensional columns of dots, when separated by 28 nm GaAs layers. Since then, a lot of effort has been spent on the understanding and the experimental realization of vertical stacking of QDs. When the dots are so closely stacked that they couple quantum mechanically, such stacks are sometimes called "artificial molecules" [16].

Xie *et al*. [108] reported that InAs/GaAs layers were vertically correlated when separated by 11 nm, the correlation starting to decrease at around 30 nm, and when the layers were separated by more than 60 nm, the correlation was essentially gone. The authors derived a one-dimensional model based on gradients in the surface chemical potential to explain the phenomenon. It was argued that by growth of a compressively/*tensile* strained layer of QDs on a substrate and then overgrowth with a thin epitaxial capping layer, a tensile/*compressive* strain field is induced in the capping layer. When a second layer of dot material is deposited,

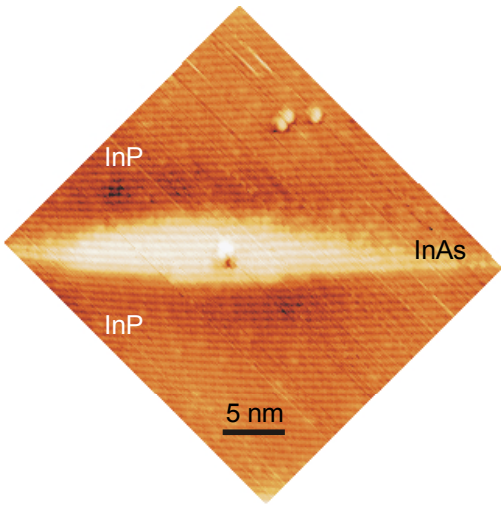

Fig. 16 High resolution, cross-sectional scanning tunneling microscope image of a single InAs/InP dot, as observed within a five-dot stack. The dot has nucleated in a depression at the InAs/InP interface, which is situated vertically above a buried dot in the previous layer (not visible in the image). The individual atoms observed are the group V, *i.e*., As and P atoms. There is no visible variation in contrast within the QDs, which indicates a composition of mainly InAs in the dots. *STM by A. Mikkelsen et al.*

mobile surface adatoms are driven by the strain field to accumulate on the capping layer above the lower lying islands. Here they reach the lower thermodynamic energy state due to the lower lattice mismatch with the capping layer in tension/*compression*. The probability of successful pairing decreases as the thickness of the capping layer is increased, since the depth of the energy minima decreases. The pairing probability depends strongly on island size [110]. In addition, if the surface does not completely planarise until the next dot layer is deposited, surface curvature effects will contribute to the selectivity.

Experimentally, the vertical correlation was found to be good between 5-40 nm in thickness for the (001) InAs/GaAs system, with a 7% lattice mismatch [108,156-158], and (001) InGaAs/GasAs [159]. Similar vertical stacking was observed also for the (001) SiGe/Si (MBE) system [160-162], and for MBE grown InP/GaInP quantum dots [163]. Kienzle *et al.* [164] found correlation between nominally pure Ge/Si island layers, which have a 4% lattice mismatch, up to 70 nm. Recently, vertical columns of dots on (001) InAs/InP (MOVPE) [12], and InAs/InGaAsP/InP (CBE) [165] were demonstrated.

Tersoff *et al.* [117] suggested that the superposition of strain fields from closely spaced buried dots could result in lateral ordering and improved size homogeneity of the dots. The overlapping of strain fields could cause one local strain minima and lead to the elimination of one of the nearby stacks, forming only one continual column. Such merging of nearby columns was observed experimentally by, for instance, Solomon *et al.* [166]. The elastic interaction of dots, in the stacks, was predicted to give rise to lateral ordering, and increased size homogeneity of the dots, theoretically [117,119,167,168] and was observed experimentally [103,163,166,169].

On the other hand, a common observation has been that the dots increase in size with following layers in a superlattice. Teichert *et al.* [103] demonstrated a change in aspect ratio of Ge/Si dots for 40 layer stacks, from a prismlike crystal shape to approximately a foursided pyramid, and an increase in the island height of a factor three. Similar effects were reported for InAs/GaAs [170-173] and InAs/InP [12] quantum dot stacks. Kienzle *et al*. [164] demonstrated that the increase in island size was more pronounced for smaller spacer layer thickness, and that no increase in island size was observed for non-correlated islands. These results indicate that the overall dot size homogeneity is not necessarily improved by vertical stacking.

For multi-layer arrays of 2D islands of CdSe/ZnSe [174], a vertical anti-correlation between islands in successive layers was observed, seeming in contradiction with the theoretical explanations of Xie *et al*. [108], and Tersoff *et al.*

[117]. In these models, the buried islands were treated as elastic point defects and the crystal was considered to be an elastically isotropic medium. The discrepancy between these theories and the experimental observation by Strassburg *et al.* [174] was explained by taking into account the elastic anisotropy found in II-VI materials [119].

The exotic $PbSe/Pb_{1-x}Eu_xTe$ system, with islands under tensile strain on (111) oriented substrates, exhibits hexagonal spatial ordering after multi layer growth [168,169]. With increasing successive layers, more than ten, an increased

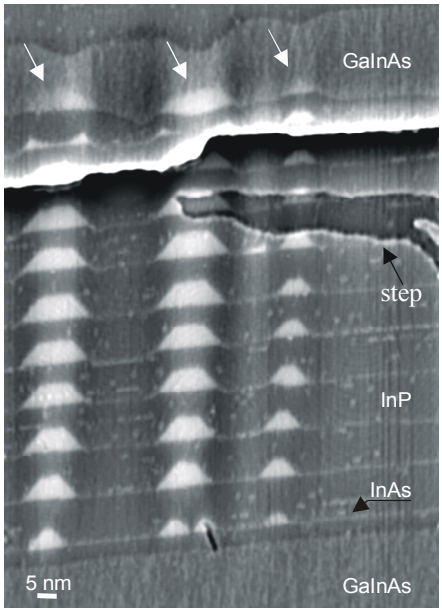

Fig. 17 X-STM image of InAs/InP ten dot stacks, the cleavage exposed is the (110) surface. The dots in the vertical stack are characterized by a (001) base and top plane. The sides are clearly faceted with an inclination of about 54° to the (001) plane, characteristic of the intersection between the {-1-1-1}B and the (001) plane. When the cleavage exposed was the (1-10) surface, 35° angles were observed, characteristic for the intersection line of the {101} side facets with a (1-10) cleavage plane. All together, this indicates that InAs/InP dots have the same symmetry as InP/GaInP QDs [175]. Not only the ten intentionally grown dots in the stack are visible, but an eleventh spontaneously formed dot (without any InAs deposit) is observed on top of the final 12 nm InP barrier directly at the InP/GaInAs interface, as indicated by the arrows (see manuscript XII).
The tenth dot in the stack has a peculiar appearance. This is most probably due to non-complete capping of InP before ramping up the temperature for further growth. Then, material from the dot can be converted by As-P exchange, and In atoms migrate off the QDs to incorporate preferentially on the wetting layer [176]. *STM by A. Mikkelsen et al.*

homogeneity in size of the dots and lateral spacing between the dots was observed. In addition, the size homogeneity between successive layers of dots was shown to be excellent under the same conditions, with no increasing size of the dots in successive layers [168,169]. The vertical ordering of these dots was observed in a face-centered cubic fashion [168,169].

Holy *et al*. [118] approximated the dots as point stress sources buried in an anisotropic semi-infinite medium, and calculated the strain energy distribution on the surface due to buried dots, to explain the vertical and lateral ordering of self assembled quantum dots, *e.g.*, vertical correlation, anti correlation, and face centered cubic like stacking of dots in the different materials. The authors [118] showed that the depth and the position of the strain energy minima at the surface are determined by the elastic anisotropy in materials. The central strain energy minimum (as modeled by Xie *et al.* [108]) is replaced by several side minima for growth along the elastically soft directions.

Materials intermixing and exchange reactions affect the properties of the grown quantum dot stacks, wetting layer, and separating spacer layer. It is commonly observed in STM investigation of the stacking phenomena that for MBE grown InAs/GaAs, In from InAs layers intermix into the growing spacer GaAs layer [166,170,173] (485 °C, 500 °C, and 512 °C), resulting in an In concentration gradient in the GaAs spacer layer. The authors observed that the In intermixing is less directly above the formed dots, indicating that the In derives mainly from the wetting layer and not from the InAs/GaAs islands. Bruls *et al*. [173] argued that the reduced indium segregation above the dots occurs because indium atoms in the dots would give up a position that is energetically favorable, for a position that is highly unfavorable under compressive strain in the GaAs. Therefore, the indium remains in the top of the dot, where the lattice constant is more comparable to that of InAs.

By cross sectional STM, it was shown that MOVPE grown stacks of InAs/GaAs (485 °C) shows much less of this materials intermixing [171,172], as compared to the MBE grown samples. Recently, the first cross sectional scanning tunneling microscope measurements on stacked (001) InAs/InP quantum dots were carried out [63] (MOVPE, 500 °C). Twofold dot stacks were formed by deposition of 1.2 ML InAs in each layer, separated by InP. The structure investigated was embedded in GaInAs, and an interesting phenomenon was observed; due to As-P exchange and possibly phase segregation of the GaInAs, spontaneously formed dots appeared on top of the grown stacks, immediately at the GaInAs/InP interface, even though no InAs was deposited.

Xie *et al.* [108] reported the complete planarisation of the GaAs spacer layer above InAs/GaAs islands with average heights of 3.5 nm, before deposition of following dot layers. In the InAs/InP system, with average dot heights of about 6 nm, the surface often shows small depressions in the InP surface just above a buried stack, after 15 nm InP deposition. Something that, in addition to the strain related part adds to the selectivity of dot positioning.

Recently, anti-correlated ordering was observed for the III-V materials [177,178], where InAs was embedded in InAlAs on (001) InP (MBE, 470-530 °C). Brault *et al.* [178] suggested that In phase segregates from the InAlAs to form In-rich V-like features, originating from the side facets of the dots, which propagate through the InAlAs spacer layer, thus forming Al rich material between the seed dots. Surface curvature effects probably add to the selectivity in these experiments, since in TEM images from the structures it is visible that the surface did not planarise between successive layers. The dots were found in the deepest depressions that are situated in-between the buried dots.

The combination of surface patterning and local strain fields was used by Schmidt *et al.* [179] to produce highly ordered arrays of Ge islands on strained-layer Si superlattice templates.

4. Imaging techniques

4.1 Introduction

The need for high-resolution microscopy is obvious, since, for example, InAs dots have heights of about 6 to 8 nm and widths of about 20 to 30 nm [180] [125]. Scanning probe microscopy and electron beam microscopy are complementary characterization tools. Commonly, scanning probe methods are used for topographic imaging, while scanning electron microscopy is more suitable to determine the shape of larger 3D objects or doping profiles, for instance.

4.2 Scanning probe microscopy

Atomic force microscopy (AFM) is a tool used to study nanoscale structures on conducting as well as insulating surfaces. It uses a tip that is mounted at the edge of an elastic cantilever. In the non-contact mode (of distances greater than 10Å between the tip and the sample surface), Van der Waals, electrostatic, magnetic or capillary forces produce images of topography, whereas in the contact mode, the force is repulsive due to the Pauli exclusion principle. During this work, the AFM has been used with the tip either touching the sample (contact mode), or the tip tapping across the surface (tapping mode) much like the cane of a blind person.

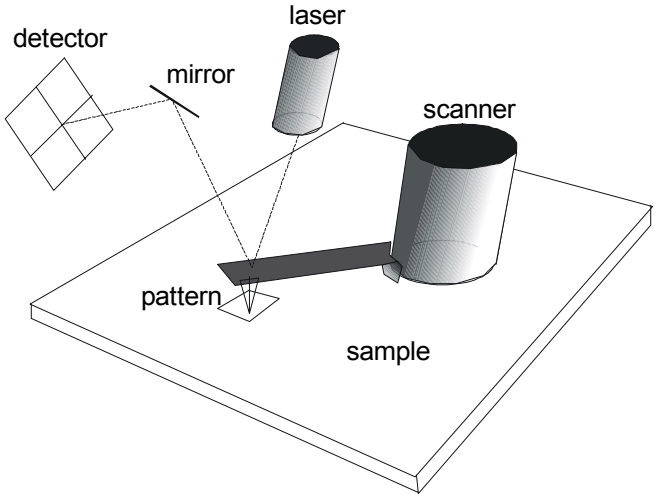

Fig. 18 Schematic of an atomic force microscopy set-up

Changes in the forces, *i.e.*, the tip-sample distance will cause changes in the deflection of the cantilever. The changes are usually recorded by a position sensitive photo-detector via a reflected laser beam, which is focused at the cantilever. A feedback loop is used to keep the deflection of the cantilever and thus the position of the reflected beam constant, by adjusting the sample in z-direction while it is scanned in the *x*, *y*-plane. A topographical image can be reconstructed from the adjustments in z-direction made during the *x*-*y* scan.

The lateral resolution obtainable in AFM is limited by the sharpness of the tip, in combination with the geometry of the measured object [181]. Tip-sample interactions must always be taken into account for a correct interpretation of AFM images. A wide tip will detect a particle more often in the scanning procedure than a very sharp one and hence the apparent size of the studied object is enlarged by the size of the tip. A standard AFM tip has a tip radius of 50 nm and is shaped like a pyramid with a base of 4×4 μm^2 and a height of 4 µm. Extremely sharp AFM tips have been obtained by electron beam deposition of a carbon whisker at the tip edge of a conventional AFM tip [83]. The topographical resolution is determined by the sensitivity of the piezoelectric elements in combination with the stability of the instrument and can go below 1Å.

Scanning tunneling microscopy (STM) is another similar approach where the surface is scanned with a very sharp tip, although in this case a metal tip is brought

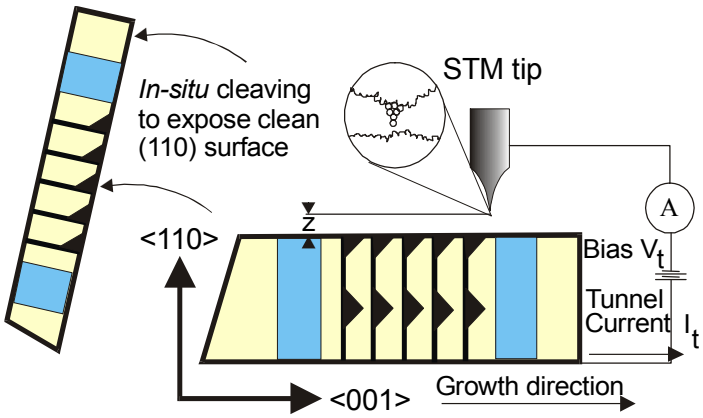

Fig. 19 Schematic of a cross-sectional scanning tunneling microscopy setup, *z* is the distance between tip-sample, and I_t is the tunneling current from tip-sample, which is measured and kept constant. In order to keep the current constant while scanning, the tip is either retracted from, or lowered closer to the surface, by the use of a piezo-element, in dependence on surface morphology and surface electronic structure.

into close proximity to a conductive specimen. The sharp conducting tip is brought close to the surface of a conducting sample and a voltage is applied between the tip and the sample. If the distance between the tip and surface is small enough, electrons can tunnel across the gap, generating a current. The tunneling probability for an electron across the gap depends exponentially on the width of the barrier. A small change in gap width thus leads to a large change in the tunneling current. The most common way of operating the STM is to keep the current constant in each measurement point by adjusting the tip sample distance at the same time as the tip is scanned over the surface. The tip height displacement is displayed as a function of position, providing an image of the corresponding surface "topography" [181].

During STM measurements, the use of an UHV system reduces the amount of contamination caused by native oxides. In cross-sectional STM [182], the ability of *in-situ* cleaving is especially useful, since then the surface will not be exposed to air, and contaminations will be minimized before characterization.

4.3 Electron beam microscopy

Electron microscopy is based on the interaction between the sample and a focused electron beam. Since the de Broglie wavelength of electrons is much lower than the wavelength of visible light, the resolution is correspondingly higher for electron

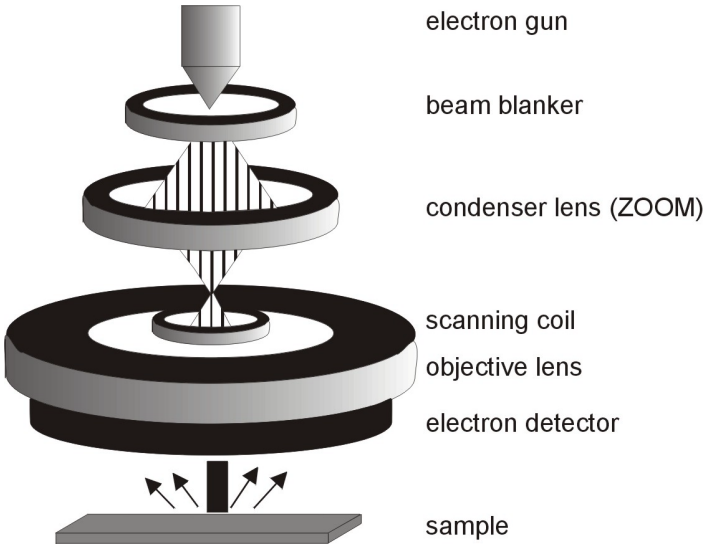

Fig. 20 Schematic of a scanning electron microscopy setup

microscopical methods than for optical microscopy. The most widely used methods are transmission electron microscopy (TEM) and scanning electron microscopy (SEM).

In SEM, the sample to be investigated is fixed on a sample holder and inserted into the microscopes vacuum chamber. An electron gun emits electrons, which are accelerated by an externally applied voltage towards the surface. The beam, which scans the surface, is focused to a small spot by sets of magnetic electron lenses. When the electrons are scattered on the sample, an image can be obtained from the secondary electrons.

5 Summary of papers

Paper I, II, and VII (*In-situ* growth of self-assembled quantum dots)

The InAs/InP system is interesting since its emission is close to 1.55 μm, which is well suited for fiber optical transmission. One possible application is therefore a quantum dot laser with a low threshold current and high modulation speed for use in fiber optical systems. The low emission energy of the dots was, from an experimental point of view, a problem since an ordinary silicon based CCD camera has a cut off wavelength of about 1 μm, which would not be suitable for detection of emission from these dots. Therefore, the measurements were performed on a Fourier transform infrared spectrometer (FTIR) with an InSb detector. The spatial resolution of this system is in the order of mm, and no single dot studies were possible.

Paper I. Room temperature operation is of great importance for device applications. We reported on optical investigations of InAs/InP quantum dots up to room temperature. The luminescence was found to be strong even at room temperature, which is due to the large band offsets in the type-I InAs/InP heterostructure. In this study, it was also possible to observe luminescence from excited states. My contribution was MOVPE growth.

Paper II. In this paper, the effects of substrate doping and surface morphology on densities and sizes of self assembled InAs/(001)InP islands were investigated. Used substrates were n-doped InP:Sn and semi insulating InP:Fe. The islands were deposited either on well-defined terraced surface with monolayer high steps grown at 650 °C or on rougher surfaces prepared at lower temperatures, 500 °C. The island density was significantly higher on the rough surfaces and the Fe doped substrates, as compared to the terraced surfaces and the Sn doped substrates, under otherwise identical deposition conditions. The explanation for the different densities on rough and terraced structures is that the diffusion length is shorter on a rough surface. Since the inter-island distance follows the surface diffusion length, nucleation on a rough surface leads to higher densities. Concerning the substrate doping dependence, we could not give a solid explanation. However some effects of doping that could affect the island density were proposed. Charge accumulation at the surface, migration of dopants towards the growing surface, or different

thermal conductivity of the Sn and Fe doped substrates leading to different surface temperatures. The main conclusion of this paper was that InAs/InP island formation is very sensitive to substrates and substrate preparation. My contributions were to plan the experiments, grow the samples, AFM characterization, and writing the paper.

Paper VII. In this study, InAs QDs were grown on InGaAlAs layers, lattice matched to InP, with varied Al content. The idea was that the luminescence from the dots might be tunable with varied Al content. We were hoping for a drastically reduced size of the dots, when introducing Al in the layers. It turned out, however, that the emission wavelength of the dots grown was rather long, around 2 μm, with a rather broad full width at half maximum value, about 77 meV. At the highest Al content, the dots were the smallest and luminesced at 1.99 μm. Step bunching of the layers was observed, and dots nucleated selectively at steps of the terraces. My contributions were planning the experiments, some of the MOVPE growth runs, AFM characterization, assisting in PL measurements, and writing the paper.

Paper III, V and VI (resonant tunneling through self-assembled quantum dots)

Investigations on tunneling phenomena through QDs are interesting because they promise new knowledge about transport in low dimensional systems, and such investigations will hopefully lead to new interesting devices. All previous investigations on resonant tunneling through self-assembled quantum dots have been done on devices containing a large number of QDs. This is important to keep in mind since the results differ qualitatively from those expected from a single dot or a single dot stack.

In paper III, results of electrical characterization on stacked InAs/InP quantum dots were presented. The density of freestanding dots was observed by AFM to be 4×10^{6} cm^{-2}, and measurements were performed on low-density GaInAs/InP/InAs/InP/GaInAs QD stacks formed by depositing two layers of 0.3 ML InAs, separated by 15 nm InP. Thus we expected a macroscopic contact, of 63×63 μm^{2}, to cover less than 150 stacks. Sharp resonant tunneling features with high peak to valley ratios were observed through the stacks, due to resonance occurring only if the zero-dimensional states in the two dots align energetically at the same time as emitter states and collector states for supplying and receiving tunneling electrons are available, respectively. Negative differential resistance in the structures was observed up to a point above the temperature for liquid nitrogen.

The size homogeneity of the dots was observed as a broad main feature with sharp current peaks superimposed on it. My contributions were to plan the experiments, grow the structures, AFM characterization, assistance on electrical measurements, and writing main part of the paper.

For paper V and VI, we used a number of experimental techniques such as electron beam lithography (EBL), optical lithography and etching to make feasible the realization of small contact sizes down to 2×2 μm^2, which is in the order of the density of quantum dots. The aim was to isolate as few QDs as possible beneath a contact, in order to study tunneling through single dots or single dot stacks.

In paper V, we compared resonant tunneling through a single layer of InAs/InP QDs and two-dot stacks of quantum dots. The tunneling was observed over a certain range of bias, which was compared with the full width at half maximum value of PL spectra measured on a similar dot structure, to obtain a voltage to energy conversion factor of 0.09 eV/V. The difference observed between tunneling through single dot layers and double dot layers was viewed as going from a two-dimensional emitter to a zero-dimensional emitter. The temperature dependence of the tunneling experiments showed the broadening of the onset of an isolated resonant tunneling peak for a single dot layer, on the order of kT, whereas the double dot layer was almost unaffected as the temperature was increased from 0.3 to 12 K, indicating the smearing of the Fermi surface for the two dimensional emitter, and the zero dimensional nature of the emitter state, as provided by the larger (upper) dot in a stack. My contributions were MOVPE growth of the structures, discussions, and assistance with electrical measurements.

In paper VI, the temperature dependence on tunneling through stacked quantum dots was carefully studied. The main result was the observation of a temperature-activated peak that appeared at the low bias side of an isolated single stack resonant tunneling peak. This was explained as tunneling through a doubly charged state in the first dot, where the Coulomb charging energy separates the doubly charged state from the singly charged state. The Coulomb charging energy was calculated by a parallel plate approximation to be about 8 meV, which was in good agreement with the appearance of the temperature-activated peak, using a voltage to energy conversion factor of 0.1eV/V. For these tunneling diodes, peak to valley ratios of up to 1300 were readily achieved, a value which can be compared to tunneling through our optimized two dimensional quantum well structures with peak to

valley ratios of up to 5 [183], in the GaAs/GaAsP materials system. My contributions were MOVPE growth of the structures and discussions.

Paper IV, VIII, and IX (lateral site control of self assembled quantum dots structures)

To order dots on the semiconductor surface is important from a device point of view. During the work of these papers, the main goal has been to develop a method to make feasible the spatial control of a resonant tunneling quantum dot stack.

In paper IV, we report on a novel method for laterally controlling the position of dots. Electron beam induced carbon deposition was used to deposit carbon nano-growth masks at the surface. The growth masks were partially overgrown and then selectively removed, *ex-situ*, leaving a patterned surface. The growth of InAs on such a patterned surface resulted in selective quantum dot growth, in and around the patterns. We found that annealing of the surface under an arsine ambient, provided enough material for dots to be formed in the holes by As-P exchange reactions. My contributions were to plan and perform all experiments, characterization, and writing the paper.

In paper VIII, the As-P exchange reactions, providing material for dot material were studied. The effect of temperature and annealing time of the patterned surface under arsine containing ambient, on the yield of dots in the holes was reported. Temperatures used were 500, 520 and 540 °C. The higher the temperature, the higher the yield of dots in the holes and the stronger the As-P exchange reactions. Annealing times were 30 s, 1 min and 3 min. With increasing annealing times, the surface tended to planarize. It was argued that the planarization occurred as a consequence of the topmost epitaxial layers being alloyed by the procedure together with adatom diffusion into the holes.

Furthermore, the effect of capping randomly distributed InAs dots with InP was studied by TEM and IV-characterization. It was found that more material for dot formation was incorporated during capping, due to carry over effects. The density of capped dots was about 100 times higher, as compared to the density of the freestanding. My contributions were to plan the experiments, MOVPE growth, processing for the site control method, AFM characterization, and writing the paper.

In paper IX, the transfer of the site control method to the SiGe/Si system was investigated, with the difference that in this case, the growth masks were never removed, but partially overgrown. It was shown that quadruples of SiGe quantum dots nucleated preferentially in pits positioned at the surface. By increasing the size of the carbon growth mask, and thereby making the lateral extension of the pit larger, more dots formed around the pit. Pyramids were formed around the pits, which by deposition of more material could be converted into domes (in more detailed investigations [184], we often found pyramidal islands elongated in <100> in the pits). The results were discussed in terms of surface curvature and effective strain relaxation. My contributions were planning, discussions, processing for the site control method, AFM characterization, and writing parts of the paper.

Paper X, (vertical stacking of quantum dots)

In this study, we reported on cross sectional scanning tunneling microscopy on the cleavage of a sample with InAs/InP quantum dot stacks. We investigated a structure similar to the one previously reported on resonant tunneling through. It was found that the dots aligned vertically on top of each other, due to the strain field induced by lower lying dots. The InAs quantum dots were mainly pure InAs, and not severely alloyed $InAs_xP_{1-x}$. A spontaneously formed dot at the InP/GaInAs interface on top of the stacks, where no InAs was deposited, was observed in about 2/3 of the stacks. The effect was discussed in terms of phase segregation effects of the GaInAs and enhanced As-P exchange at the strained regions. My contributions were MOVPE growth, and writing parts of the paper.

Paper XI, and XII (growth of one dimensional nano-whiskers)

In paper XI, we reported on VLS growth of GaAs nano whiskers on (-1-1-1)B GaAs substrates in MOVPE. By varying the growth temperature and measuring the length of the nano-whiskers grown, we found a maximum in the whisker growth rate at about 450–475 °C. We found an Arrhenius activation energy of about 67–75 kJ/mol for the process, a value which is in agreement with activation energies reported for low-temperature planar growth of GaAs from TMG and AsH_3 on (-1-1-1)B GaAs substrates. Experimental results when varying the TMG molar fraction indicated that it is not the reaction at the (-1-1-1)B/(Au,Ga)-interface which limits the whisker growth rate, but the processes outside the Au droplet. Therefore the main conclusion of the paper is that the catalyzing Au particles act as local

catalysts only. My contributions were MOVPE growth, SEM characterization, and writing parts of the paper.

In paper XII, we reported on a method to control the sites of nano-whiskers. Electron beam lithography and metal lift-off were used to form Au disks on the surface in desired patterns. Vertical InP<-1-1-1>B nano-whiskers were then grown, in the VLS growth mode, from the gold particles deposited on the InP(-1-1-1)B surface. The lithographic nature of the method allowed individual control over the position of each nano-whisker. My contributions were discussions, and assistance in MOVPE growth.

References

[1] R. A. Smith, *Semiconductors, 2nd ed.,* (London, 1979).
[2] S. M. Sze, *Semiconductor Devices Physics and Technology* (1985).
[3] U. Kaufmann, M. Kunzer, K. Köhler, H. Obloh, W. Pletschen, P. Schlotter, R. Schmidt, J. Wagner, A. Ellens, W. Rossner, M. Kobusch, Phys. Stat. Sol. (a) 188 (2001) 143.
[4] J. Bardeen,W. H. Brattain, Physical Review 74 (1948) 230.
[5] W. Shockley, Bell System Technical Journal 28 (1949) 435.
[6] G. Moore, Electronics 38 (1965).
[7] C. Weisbuch,B. Vinter, *Quantum Semiconductor Structures: Fundamentals and Applications* (New York, 1991).
[8] J. N. Randall, M. A. Reed, R. J. Matyi, T. M. Moore, J. Vac. Sci. Technol. B 6 (1988) 1861.
[9] M. A. Reed, J. N. Randall, R. J. Aggarwal, R. J. Matyi, T. M. Moore, A. E. Wetsel, Phys. Rev. Lett. 60 (1988) 535.
[10] M. Borgstrom, T. Bryllert, B. Gustafson, J. Johansson, T. Sass, L.-E. Wernersson, W. Seifert, L. Samuelson, J. Electron. Mater. 30 (2001) 482.
[11] L. L. Chang, L. Esaki, R. Tsu, Appl. Phys. Lett. 24 (1974) 593.
[12] M. Borgstrom, T. Bryllert, T. Sass, B. Gustafson, L.-E. Wernersson, W. Seifert, L. Samuelson, Appl. Phys. Lett. 78 (2001) 3232.
[13] T. Bryllert, M. Borgstrom, L. E. Wernersson, W. Seifert, L. Samuelson, Applied Physics Letters 82 (2003) 2655.
[14] I. E. Itskevich, T. Ihn, A. Thornton, M. Henini, T. J. Foster, P. Moriarty, A. Nogaret, P. H. Beton, L. Eaves, P. C. Main, Phys. Rev. B 54 (1996) 16401.
[15] M. Narihiro, G. Yusa, Y. Nakamura, T. Noda, H. Sakaki, Appl. Phys. Lett. 70 (1997) 105.
[16] T. Bryllert, M. Borgstrom, T. Sass, B. Gustafson, L. Landin, L.-E. Wernersson, W. Seifert, L. Samuelson, Appl. Phys. Lett. 80 (2002) 2681.
[17] W. B. Garnett, Phys. Rev. B 44 (1991) 3064.
[18] N. Carlsson, T. Junno, L. Montelius, M.-E. Pistol, L. Samuelson, W. Seifert, J. Cryst. Growth 191 (1998) 347.
[19] L. Landin, M. Borgström, M. Kleverman, M.-E. Pistol, L. Samuelson, W. Seifert, X. H. Zhang, Thin Solid Films 364 (2000) 161.
[20] H. Marchand, P. Desjardins, S. Guillon, J.-E. Paultre, Z. Bourgrioua, R.-F. Yip, R. A. Masut, Appl. Phys. Lett. 71 (1997) 527.
[21] H. Petterson, C. Pryor, L. Landin, M.-E. Pistol, N. Carlsson, W. Seifert, L. Samuelson, Phys. Rev. B 61 (1999) 4795.
[22] M. Holm, M. E. Pistol, C. Pryor, Journal of Applied Physics 92 (2002) 932.
[23] S. Lourdudoss,O. Kjebon, Ieee Journal of Selected Topics in Quantum Electronics 3 (1997) 749.
[24] G. B. Stringfellow, *Organometallic Vapor-Phase Epitaxy: Theory and Practice* (Academic Press, Inc., London, 1989).
[25] B. S. Meyerson, Proceedings of the Ieee 80 (1992) 1592.
[26] J. S. Foord, G. J. Davies, W. T. Tsang, *Chemical Beam Epitaxy and Related Techniques* (John Wiley & Sons Ltd, Chichester, 1997).

[27] J. Y. Tsao, *Materials Fundamentals of Molecular Beam Epitaxy* (Academic Press, London, 1993).
[28] G. B. Stringfellow, *Organometallic Vapor-Phase Epitaxy: Theory and Practice*, Second Edition ed. (Academic Press, Inc., 1999).
[29] D. W. Kisker, T. F. Kuech, (Elsevier Science, Amsterdam) (1993) 93.
[30] B. S. Meyerson, Appl. Phys. Lett. 48 (1986) 797.
[31] D. W. Greve, Mat. Sci. Eng.B 18 (1993) 22.
[32] H. M. Manasevit, W. I. Simpson, J. Electrochem. Soc 13/14 (1968) 156.
[33] E. Bauer, Zeitschr. Kristallographie 110 (1958) 277.
[34] F. C. Frank, J. H. V. d. Merwe, Proc. R. Soc. London Ser. A 198 (1949) 205.
[35] I. N. Stranski,L. Krastanow, Sitz.Ber.Akad.Wiss., Math.-naturwiss. Kl.Abt.IIb 146 (1938) 797.
[36] M. Volmer,A. Weber, Z. Physik. Chem. 119 (1926) 277.
[37] L. Goldstein, F. Glas, J. Y. Marzin, M. N. Charasse, G. L. Roux, Appl. Phys. Lett 47 (1985) 1099.
[38] W. Seifert, N. Carlsson, M. Miller, M.-E. Pistol, L. Samuelson, L. R. Wallenberg, Prog. Crystal. Growth and charact 33 (1996) 423.
[39] D. Walton, J. Chem. Phys 37 (1962) 2182.
[40] P. Chen, Q. Xie, A. Madhukar, L. Chen, A. Konkar, J. Vac. Sci. Technol. B12 (1994) 2568.
[41] G. S. Solomon, J. A. Trezza, J. J S Harris, Appl. Phys. Lett. 66 (1995) 991.
[42] M. Sopanen, H. Lipsanen, J. Ahopelto, Appl. Phys. Lett. 67 (1995) 3768.
[43] R. E. Welser, L. J. Guido, Appl. Phys. Lett. 68 (1996) 912.
[44] J. Johansson, N. Carlsson, W. Seifert, Physica E 2 (1998) 667.
[45] A. L. Barabasi, H. E. Stanley, University Press, Cambridge (1995).
[46] J. Johansson, W. Seifert, V. Zwiller, T. Junno, L. Samuelson, Appl. Surf. Sci. 134 (1998) 47.
[47] M. Grundmann, Physica E 5 (2000) 167.
[48] J. Hergeth, D. Grutzmacher, F. Reinhardt, P. Balk, Journal of Crystal Growth 107 (1991) 537.
[49] A. Watanabe, T. Isu, M. Hata, Y. Katayama, Journal of Crystal Growth 115 (1991) 371.
[50] G. Hollinger, D. Gallet, C. Gendry, C. Santinelli, P. Viktorovitch, J. Vac. Sci. Technol. B 8 (1990) 832.
[51] C. Walther, W. Hoerstel, H. Niehus, J. Erxmeyer, W. T. Masselink, J. Cryst. Growth 209 (2000) 572.
[52] V. Sobiesierski, V. Westwood, P. J. Parbrook, K. B. Ozanyan, M. Hopkinson, C. R. Whitehouse, Appl. Phys. Lett. 70 (1997) 1423.
[53] W. Seifert, D. Hessman, X. Liu, L. Samuelson, J. Appl. Phys. 75 (1993) 1501.
[54] L. Samuelson, W. Seifert, in *Handbook of crystal growth*; *Vol. 3b*, edited by D. T. J. Hurle (Elsevier Science, Amsterdam, 1994).
[55] E. Bergignat, M. Gendry, G. Hollinger, G. Grenet, Physical Review B 49 (1994) 13542.
[56] M. Taskinen, M. Sopanen, H. Lipsanen, J. Tulkki, T. Tuomi, J. Ahopelto, Surf. Sci. 376 (1997) 60.
[57] S. Yoon, Y. Moon, T.-W. Lee, E. Yoon, Appl. Phys. Lett. 74 (1999) 2029.

[58] B. Wang, F. Zhao, Y. Peng, Z. Jin, Y. Li, S. Liu, Appl. Phys. Lett 72 (1998) 2433.
[59] P. J. Poole, R. L. Williams, J. Lefebvre, S. Moisa, J.Cryst. Growth 257 (2003) 89.
[60] M. Borgstrom, J. Johansson, W. Seifert, L. Samuelson, Appl. Phys. Lett 78 (2001) 1367.
[61] J. Lefebvre, P. J. Poole, J. Fraser, G. C. Aers, D. Chithrani, R. L. Williams, J. Cryst. Growth 234 (2002) 391.
[62] M. Borgstrom, T. Bryllert, T. Sass, L.-E. Wernersson, L. Samuelson, W. Seifert, J. Cryst. Growth 248 (2003) 310.
[63] M. Borgstrom, A. Mikkelsen, L. Ouattara, E. Lundgren, L. Samuelson, W. Seifert, Appl. Phys. Lett. (2003) submitted.
[64] V. Magidson, D. V. Regelman, R. Beserman, K. Dettmer, Applied Physics Letters 73 (1998) 1044.
[65] G. Capellini, M. De Seta, F. Evangelisti, Applied Physics Letters 78 (2001) 303.
[66] A. Rosenauer, U. Fischer, D. Gerthsen, A. Forster, Appl. Phys. Lett. 71 (1997) 3868.
[67] I. Kegel, T. H. Metzger, A. Lorke, J. Peisl, J. Stangl, G. Bauer, J. M. Garcia, P. M. Petroff, Phys. Rev. Lett. 85 (2000) 1694.
[68] P. B. Joyce, T. J. Krzyzewski, G. R. Bell, B. A. Joyce, T. S. Jones, Phys. Rev. B 58 (1998) 15981.
[69] R. S. Wagner, W. C. Ellis, Appl. Phys. Lett. 4 (1964) 89.
[70] R. S. Wagner, in *Whisker technology*, edited by A. P. Levitt (Wiley, New York, 1970), p. 47.
[71] L. Samuelson, J. Lindahl, L. Montelius, M. E. Pistol, Phys. Scripta T42 (1992) 149.
[72] S. S. Fan, M. G. Chapline, N. R. Franklin, T. W. Tombler, A. M. Cassell, H. J. Dai, Science 283 (1999) 512.
[73] K. Hiruma, M. Yazawa, T. Katsuyama, K. Ogawa, K. Haraguchi, M. Koguchi, H. Kakibayashi, J. Appl. Phys. 77 (1995) 447.
[74] K. Haraguchi, K. Hiruma, K. Hosomi, M. Shirai, T. Katsuyama, in *J. Vac. Sci. Technol. B*; *Vol. 15* (1997), p. 1685.
[75] A. K. Viswanath, K. Hiruma, M. Yazawa, K. Ogawa, T. Katsuyama, Microw. Opt. Techn. Lett. 7 (1994) 94.
[76] M. Yazawa, M. Koguchi, K. Hirutna, Appl. Phys. Lett. 58 (1991) 1080.
[77] Y. F. Chan, X. F. Duan, S. K. Chan, I. K. Sou, X. X. Zhang, N. Wang, Appl. Phys. Lett. 83 (2003) 2665.
[78] M. Borgstrom, K. Deppert, L. Samuelson, W. Seifert, J. Cryst. Growth in press (2003).
[79] B. J. Ohlsson, M. T. Bjork, M. H. Magnusson, K. Deppert, L. Samuelson, L. R. Wallenberg, Appl. Phys. Lett. 79 (2001) 3335.
[80] M. H. Magnusson, K. Deppert, J. O. Malm, J. O. Bovin, L. Samuelson, Nanostruct. Mater. 12 (1999) 45.
[81] T. Shimada, K. Hiruma, M. Shirai, M. Yazawa, K. Haraguchi, T. Sato, M. Matsui, T. Katsuyama, Superlattice. Microst. 24 (1998) 453.
[82] T. Mårtensson, M. Borgström, B. J. Ohlsson, W. Seifert, L. Samuelson, Nanotech. (2003) in press.
[83] T. Junno, Thesis, Lund University, 1999.
[84] A. M. Morales, C. M. Lieber, Science 279 (1998) 208.

[85] D. P. Yu, Z. G. Bai, Y. Ding, Q. L. Hang, H. Z. Zhang, J. J. Wang, Y. H. Zou, W. Qian, G. C. Xiong, H. T. Zhou, S. Q. Feng, Appl. Phys. Lett. 72 (1998) 3458.
[86] Y. Cui,C. M. Lieber, Science 291 (2001) 851.
[87] Y. Y. Wu, R. Fan, P. D. Yang, Nano Letters 2 (2002) 83.
[88] X. F. Duan, Y. Huang, Y. Cui, J. F. Wang, C. M. Lieber, Nature 409 (2001) 66.
[89] M. T. Bjork, B. J. Ohlsson, T. Sass, A. I. Persson, C. Thelander, M. H. Magnusson, K. Deppert, L. R. Wallenberg, L. Samuelson, Appl. Phys. Lett. 80 (2002) 1058.
[90] Y. Huang, X. F. Duan, Y. Cui, C. M. Lieber, Nano Letters 2 (2002) 101.
[91] R. Solanki, J. Huo, J. L. Freeouf, B. Miner, Appl. Phys. Lett. 81 (2002) 3864.
[92] M. S. Gudiksen, L. J. Lauhon, J. Wang, D. C. Smith, C. M. Lieber, Nature 415 (2002) 617.
[93] M. T. Bjork, B. J. Ohlsson, T. Sass, A. I. Persson, C. Thelander, M. H. Magnusson, K. Deppert, L. R. Wallenberg, L. Samuelson, Nano Letters 2 (2002) 87.
[94] B. J. Ohlsson, M. T. Bjork, A. I. Persson, C. Thelander, L. R. Wallenberg, M. H. Magnusson, K. Deppert, L. Samuelson, Physica E 13 (2002) 1126.
[95] M. T. Bjork, B. J. Ohlsson, C. Thelander, A. I. Persson, K. Deppert, L. R. Wallenberg, L. Samuelson, Appl. Phys. Lett. 81 (2002) 4458.
[96] D. V. Averin,K. K. Likharev, J. Low. Temp. Phys. 62 (1986) 345.
[97] S. D. Franceschia, J. A. Dam, E. P. A. M. Bakkers, L. F. Feiner, L. Gurevich, L. P. Kouwenhoven, Appl. Phys. Lett. 83 (2003) 344.
[98] C. Thelander, T. Martensson, M. T. Bjork, B. J. Ohlsson, M. W. Larsson, L. R. Wallenberg, L. Samuelson, Appl. Phys. Lett. 83 (2003) 2052.
[99] A. O. Orlov, I. Amlani, G. H. Bernstein, C. S. Lent, G. L. Snider, Science 277 (1997) 928.
[100] P. Mazumder, S. Kulkarni, M. Bhattacharya, J. P. Sun, G. I. Haddad, Proc IEEE 86 (1998) 664.
[101] T. T. Ngo, R. S. Williams, Appl. Phys Lett 66 (1995) 1906.
[102] C. Lee, A. L. Barabasi, Appl. Phys. Lett 73 (1998) 2651.
[103] C. Teichert, M. G. Lagally, L. J. Peticolas, J. C. Bean, J. Tersoff, Phys. Rev. B 53 (1996) 16334.
[104] J. Johansson, PhD Thesis, Lund University, 2000.
[105] C. Herring, in *The Pysics of powder metallurgy*, edited by W. E. Kingston (McGraw-Hill, New York, 1951), p. 143.
[106] D. J. Srolovitz, Acta. Metall. 37 (1988) 621.
[107] D. E. Jesson, S. J. Pennycook, J.-M. Baribeau, D. C. Houghton, Phys. Rev. Lett 71 (1993) 1744.
[108] Q. Xie, A. Madhukar, P. Chen, N. P. Kobayashi, Phys. Rev. Lett 75 (1995) 2542.
[109] G. Biasiol, E. Kapon, Phys. Rev. Lett 81 (1998) 2962.
[110] G. Springholz, M. Pinczolits, V. Holy, S. Zerlauth, I. Vavra, G. Bauer, Physica E 9 (2001) 149.
[111] M. Ozdemir, A. Zangwill, J. Vac. Sci. Technol. A 10 (1991) 684.
[112] G. Biasiol, A. Gustafsson, K. Leifer, E. Kapon, Physical Review B 65 (2002).
[113] A. Kley, P. Ruggerone, M. Scheffler, Phys. Rev. Lett. 79 (1997) 5278.
[114] E. Penev, P. Kratzer, M. Scheffler, Physical Review B 6408 (2001).
[115] G. Jin, J. L. Liu, S. G. Thomas, Y. H. Luo, K. L. Wang, B. Nguyen, Appl. Phys. Lett. (1999) 2752.

[116] M. Borgstrom, V. Zela, W. Seifert, Nanotechnology 14 (2003) 264.
[117] J. Tersoff, C. Teichert, M. L. Lagally, Phys. Rev. Lett. (1996) 1675.
[118] V. Holy, G. Springholz, M. Pinczolits, G. Bauer, Phys. Rev. Lett. 83 (1999) 356.
[119] V. A. Shchukin, D. Bimberg, V. G. Malyshkin, N. N. Ledentsov, Phys. Rev. B 57 (1998) 12262.
[120] C. Pryor, J. Kim, L. W. Wang, A. J. Williams, A. Zunger, J. Appl. Phys 83 (1998) 2548.
[121] D. Leonard, K. Pond, P. M. Petroff, Phys. Rev. B 50 (1994) 11687.
[122] M. Borgström, J. Johansson, L. Landin, W. Seifert, Appl. Surf. Sci 165 (2000) 245.
[123] M. Kitamura, M. Nishioka, J. Oshinowo, Y. Arakawa, Appl. Phys. Lett. 66 (1995) 3663.
[124] J. M. Moison, L. Leprince, F. Barthe, F. Houzay, N. Lebouche, J. M. Gerard, J. Y. Marzin, Applied Surface Science 92 (1996) 526.
[125] S. Ruvimov, P. Werner, K. Scheerschmidt, U. Gösele, J. Heydenreich, U. Richter, N. N. Ledentsov, M. Grundmann, D. Bimberg, V. M. Ustinov, A. Y. Egorov, P. S. Kop'ev, Z. I. Alferov, Phys. Rev. B 51 (1995) 14766.
[126] Y. H. Xie, S. B. Samavedam, M. Bulsara, T. A. Langdo, E. A. Fitzgerald, Appl. Phys. Lett 71 (1997) 24.
[127] T. Mano, R. Notzel, G. J. Hamhuis, T. J. Eijkemans, J. H. Wolter, Applied Physics Letters 81 (2002) 1705.
[128] O. G. Schmidt, C. Deneke, S. Kiravittaya, R. Songmuang, H. Heidemeyer, Y. Nakamura, R. Zapf-Gottwick, C. Muller, N. Y. Jin-Phillipp, Ieee Journal of Selected Topics in Quantum Electronics 8 (2002) 1025.
[129] H. Heidemeyer, S. Kiravittaya, C. Muller, N. Y. Jin-Phillipp, O. G. Schmidt, Appl. Phys. Lett. 80 (2002) 1544.
[130] T. Ishikawa, S. Kohmoto, K. Asakawa, Appl. Phys. Lett. 73 (1998) 1712.
[131] D. S. L. Mui, D. Leonard, L. A. Coldren, P. M. Petroff, Appl. Phys. Lett. 66 (1995) 1620.
[132] A. Konkar, K. C. Rajkumar, Q. Xie, P. Chen, A. Madhukar, H. T. Lin, D. H. Rich, Journal of Crystal Growth 150 (1995) 311.
[133] S. Jeppesen, M. Miller, D. Hessman, B. Kowalski, I. Maximov, L. Samuelson, Appl. Phys. Lett. 68 (1996) 2228.
[134] M. Kappelt, V. Turck, D. Bimberg, H. Kirmse, I. Hahnert, W. Neumann, Journal of Crystal Growth 195 (1998) 552.
[135] J. Lefebvre, P. J. Poole, G. C. Aers, D. Chithrani, R. L. Williams, Journal of Vacuum Science & Technology B 20 (2002) 2173.
[136] Q. Xiang, S. Li, D. Wang, K. L. Wang, J. Vac. Sci. Technol. 14 (1996) 2381.
[137] T. I. Kamins, R. S. Williams, Appl. Phys. Lett. (1997) 1201.
[138] G. Jin, J. L. Liu, K. L. Wang, Appl. Phys. Lett. (2000) 3591.
[139] Z. Y. Zhong, A. Halilovic, T. Fromherz, F. Schaffler, G. Bauer, Applied Physics Letters 82 (2003) 4779.
[140] Z. Y. Zhong, A. Halilovic, M. Muhlberger, F. Schaffler, G. Bauer, Journal of Applied Physics 93 (2003) 6258.
[141] S. Kohmoto, H. Nakamura, T. Ishikawa, K. Asakawa, Appl. Phys. Lett. 75 (1999) 3488.
[142] X. Deng, M. Krishnamurthy, Phys. Rev. Lett. 81 (1998) 1473.
[143] J. L. Gray, R. Hull, J. A. Floro, Appl. Phys. Lett. 81 (2002) 2445.

[144] V. Zela, I. Pietzonka, T. Sass, C. Thelander, S. Jeppesen, W. Seifert, Physica E 13 (2002) 1013.
[145] J. Johansson, W. Seifert, J. Cryst. Growth 234 (2002) 139.
[146] B. Mutaftschiev, in *Handbook of crystal growth*; *Vol. 1a*, edited by D. T. J. Hurle (North-Holland, Amsterdam, 1993), p. 187.
[147] G. W. Yang, B. X. Liu, Phys. Rev. B 61 (2000) 4500.
[148] K. L. Lee, D. W. Abraham, F. Secord, L. Landstein, J. Vac. Sci. Technol. B 9 (1991) 3562.
[149] J. W. Sleight, R. E. Welser, L. J. Guido, M. Amman, M. A. Reed, Appl. Phys. Lett 66 (1995) 1343.
[150] H. W. P. Koops, R. Weiel, D. P. Kern, T. H. Baum, J. Vac. Sci. Technol. B 6 (1988) 477.
[151] N. Miura, T. Numaguchi, A. Yamada, M. Konagai, J.-I. Shirakashi, Jpn. Appl. Phys. 36 (1997) L 1619.
[152] P. Boggild, T. M. Hansen, C. Tanasa, F. Grey, Nanotechnology 12 (2001) 331.
[153] N. Miura, H. Ishii, A. Yamada, M. Konagai, Jpn. J. Appl. Phys Part 2-lett. 35 (1996) L1089.
[154] Y. Akama, E. Nishimura, A. Sakai, H. Murakami, J. Vac. Sci. Technol. A 8 (1990) 429.
[155] H. W. P. Koops, J. Kretz, M. Rudolph, M. Weber, G. Dahm, K. L. Lee, Jpn. Appl. Phys-Part 1 33 (1994) 7099.
[156] G. Solomon, J. A. Trezza, A. F. Marshall, J. J. S. Harris, Phys. Rev. Lett 76 (1996) 952.
[157] M. S. Miller, J. O. Malm, M. E. Pistol, S. Jeppesen, B. Kowalski, K. Georgsson, L. Samuelson, J. Appl. Phys 80 (1996) 3360.
[158] B. Legrand, J. P. Nys, B. Grandidier, D. Stievenard, A. Lemaitre, J. M. Gerard, V. Thierry-Mieg, Appl. Phys. Lett 74 (1999) 2608.
[159] A. A. Darhuber, V. Holy, J. Stangl, G. Bauer, A. Krost, F. Heinrichsdorff, M. Grundmann, D. Bimberg, V. M. Ustinov, P. S. Kopev, A. O. Kosogov, P. Werner, Applied Physics Letters 70 (1997) 955.
[160] P. Schittenhelm, C. Engel, F. Findeis, G. Abstreiter, A. A. Darhuber, G. Bauer, A. O. Kosogov, P. Werner, Journal of Vacuum Science & Technology B 16 (1998) 1575.
[161] V. Holy, A. A. Darhuber, J. Stangl, S. Zerlauth, F. Schaffler, G. Bauer, N. Darowski, D. Lubbert, U. Pietsch, I. Vavra, Physical Review B 58 (1998) 7934.
[162] A. A. Darhuber, P. Schittenhelm, V. Holy, J. Stangl, G. Bauer, G. Abstreiter, Physical Review B 55 (1997) 15652.
[163] M. K. Zundel, P. Specht, K. Eberl, N. Y. JinPhillipp, F. Phillipp, Applied Physics Letters 71 (1997) 2972.
[164] O. Kienzle, F. Ernst, M. Ruhle, O. G. Schmidt, K. Eberl, Applied Physics Letters 74 (1999) 269.
[165] C. N. Allen, P. J. Poole, P. Marshall, J. Fraser, S. Raymond, S. Fafard, Applied Physics Letters 80 (2002) 3629.
[166] G. S. Solomon, W. Wu, J. R. Tucker, J. J S Harris, Physica E 2 (1998) 709.
[167] F. Liu, S. E. Davenport, H. M. Evans, M. G. Lagally, Phys. Rev. Lett. 82 (1999) 2528.
[168] G. Springholz, M. Pinczolits, G. Bauer, V. Holy, Science 282 (1998) 734.
[169] M. Pinczolits, G. Springholz, G. Bauer, Phys. Rev. B 60 (1999) 356.
[170] W. Wu, J. Tucker, Appl. Phys. Lett. 71 (1997) 1083.

[171] H. Eisele, A. Lenz, C. Hennig, R. Timm, M. Ternes, M. Dähne, J. Cryst. Growth 248 (2003) 322.
[172] O. Flebbe, H. Eisele, T. Kalka, F. Heinrichsdorff, A. Krost, D. Bimberg, M. Dähne-Prietsch, J. Vac. Sci. Technol. B 17 (1999) 1639.
[173] D. M. Bruls, P. M. Koenraad, H. W. M. Salemink, J. H. Wolter, M. Hopkinson, M. S. Skolnick, Applied Physics Letters 82 (2003) 3758.
[174] M. Strassburg, V. Kutzer, U. W. Pohl, A. Hoffmann, I. Broser, N. N. Ledentsov, D. Bimberg, A. Rosenauer, U. Fischer, D. Gerthsen, I. L. Krestnikov, M. V. Maximov, P. S. Kop'ev, Z. I. Alferov, Appl. Phys. Lett. 72 (1998) 942.
[175] K. Georgsson, N. Carlsson, L. Samuelson, W. Seifert, L. R. Wallenberg, Applied Physics Letters 67 (1995) 2981.
[176] C. Paranthoen, N. Bertru, O. Dehaese, A. L. Corre, S. Loualiche, B. Lambert, G. Patriarche, Appl. Phys. Lett. 78 (2001) 1751.
[177] H. Li, J. Wu, Z. Wang, T. Daniels-Race, Appl. Phys. Lett. 75 (1999) 1173.
[178] J. Brault, M. Gendry, O. Marty, M. Pitaval, J. Olivares, G. Grenet, G. Hollinger, Appl. Surf. Sci. 162 (2000).
[179] O. G. Schmidt, N. Y. Jin-Phillipp, C. Lange, U. Denker, R. Schreiner, H. Grabeldinger, H. Schweizer, Appl. Phys. Lett. (2000) 4139.
[180] Y. Nabetani, T. Ishikawa, S. Noda, A. Akasaki, J. Appl. Phys. 76 (1994) 347.
[181] R. Wiesendanger, (Cambridge University press, Cambridge) (1994).
[182] R. M. Feenstra, Semicond. Sci. Tech. 9 (1994) 2157.
[183] L.-E. Wernersson, B. Gustafson, A. Gustafson, M. Borgstrom, I. Pietzonka, T. Sass, W. Seifert, L. Samuelson, Appl. Surf. Sci. 190 (2002) 252.
[184] M. Borgstrom, V. Zela, W. Seifert, J. Cryst. Growth in print (2003).